The Influence of the Inclusion of Soil Freezing on Simulations by a Soil–Vegetation–Atmosphere Transfer Scheme

A. BOONE AND V. MASSON

Météo-France/Centre National de Recherche Météorologique, Toulouse, France

T. MEYERS

Atmospheric Turbulence and Diffusion Division, National Oceanic and Atmospheric Administration, Oak Ridge, Tennessee

J. NOILHAN

Météo-France/Centre National de Recherche Météorologique, Toulouse, France

(Manuscript received 15 July 1999, in final form 23 November 1999)

ABSTRACT

The interactions between the soil, biosphere, and atmosphere (ISBA) land surface parameterization scheme has been modified to include soil ice. The liquid water equivalent volumetric ice content is modeled using two reservoirs within the soil: a thin surface layer that directly affects the surface energy balance, and a deep soil layer. The freezing/drying, wetting/thawing analogy is used, and a description of the modifications to the ISBA force–restore scheme, in particular to the hydrological and thermal transfer coefficients, is presented. In addition, the ISBA surface/vegetation scheme is coupled to a multilayer explicit diffusion soil heat and mass transfer model in order to investigate the accuracy of the force–restore formalism soil freezing parameterization as compared with a higher-order scheme.

An example of the influence of the inclusion of soil freezing in ISBA on predicted surface and soil temperatures and surface fluxes is examined using prescribed atmospheric forcing from a micrometeorological case study that includes freeze–thaw cycles. Surface temperature prediction is improved in comparison with the observed values, especially at night, primarily from the release of latent heat as the soil freezes. There is an improvement in the overall surface flux prediction, although for some specific periods there is increased error in the prediction of various components of the surface energy budget. Last, the simplified force–restore approach is found to produce surface flux and temperature predictions consistent with the higher-resolution model on typical numerical weather prediction model timescales (on the order of several days to two weeks) for this particular site.

1. Introduction

The importance of the characterization of the land surface for meteorological numerical models has been gaining attention in recent years. The Project for Intercomparison of Land Surface Parameterization Schemes (PILPS) has examined the current state of so-called Soil–Vegetation–Atmosphere Transfer (SVAT) schemes through various international intercomparison studies (Henderson-Sellers et al. 1993, 1995). Recently, PILPS has underscored the importance of modeling cold-climate land surface processes, as most land surface model validation or test studies to date have emphasized tropical and midlatitude climates. Schlosser et al. (2000) analyzed simulations by 21 research and operational SVAT schemes under the auspices of PILPS for an 18-yr off-line (driven by atmospheric forcing as opposed to being coupled to a parent atmospheric model) simulation. It was determined that the parameterization of frozen soil (or lack of such a parameterization) was a cause for considerable model disagreement in predicted soil moisture, which, in turn, was related to disparity in predicted surface fluxes. The treatment of soil freezing processes was also shown to have long-term effects on model variability.

Several studies have been recently done that specifically address the soil ice parameterizations in SVAT schemes. Slater et al. (1998) showed the importance of including soil ice processes in the Best Approximation of Surface Exchanges (BASE) SVAT scheme for climate model timescales (multiyear simulations) using off-line experiments. The degree of freezing of the soil that

Corresponding author address: Aaron A. Boone, Météo-France, CNRM/GMME/MC2, 42 avenue Coriolis, 31057 Toulouse Cedex, France.
E-mail: boone@cnrm.meteo.fr

occurred during the winter months influenced the partitioning of precipitation and/or snow meltwater into either runoff or infiltration that, in turn, affected soil moisture and surface fluxes of heat and moisture into the summer season. Cox et al. (1999) incorporated soil freezing physics into the U.K. Meteorological Office Surface Exchange Scheme (MOSES) SVAT coupled to a climate model and obtained improved atmospheric simulations for high-latitude regions, primarily from latent heat release from soil water phase changes. Giard and Bazile (2000) obtained improved forecast scores from the inclusion of a soil ice scheme in the interactions between the soil, biosphere, and atmosphere (ISBA) SVAT scheme coupled to the French operational numerical weather prediction (NWP) model ARPEGE (Action de Researche Petite Echelle Grande Echelle) (Courtier and Geleyn 1988).

ISBA is a so-called force–restore model (Deardorff 1977, 1978), in which the physics of the land surface have been simplified in an attempt to optimize the balance between the computational speed (for NWP models) and the representation of what are deemed to be the most important processes (Noilhan and Planton 1989; Noilhan and Mahfouf 1996, hereinafter referred to as NP89 and NM96, respectively). The force–restore coefficients are oftentimes calibrated using more complex or higher-resolution explicit soil schemes (e.g., Dickinson 1984; NP89; Boone et al. 1999), or the accuracy of the model solutions is examined by comparing them with those obtained using relatively high resolution models (Deardorff 1978). In the same spirit, a relatively high resolution soil model [ISBA-Diffusion (ISBA-DF)], which uses the same basic underlying physics as force–restore ISBA (ISBA-FR), is coupled to the ISBA atmospheric surface layer/vegetation scheme in order to examine how well a model using the force–restore formalism can reproduce the effects of soil ice with respect to a higher-resolution model.

This study is an extension of the work done by Giard and Bazile (2000) in that their baseline single-ice reservoir model is used but with some modifications. A more general two-layer approach is used here, because this distinction was found to be especially important for extreme cold outbreaks. The soil hydrological parameterization was also modified to account for soil freezing. This paper is divided into seven additional sections: a general review of the current representation of soil ice used by SVATs, a description of the modifications and additions required for the inclusion of soil ice into ISBA-FR, a brief description of ISBA-DF, a presentation of a case study used to demonstrate model performance, results from numerical experiments, a discussion, and conclusions.

2. Current representation of soil ice in SVATs

The representation of soil ice in SVATs is relatively simple in comparison with state-of-the-art soil models that are fully devoted to detailed soil heat and mass transfer simulations: a discussion of basic modeling approach differences between such detailed models and SVATs is given by Slater et al. (1998). The soil ice representation in SVATs can currently be broken into two rather broad categories, so-called explicit and implicit schemes.

Implicit soil ice schemes do not keep track of the actual quantity of soil ice, but rather model the effect of subfreezing soil temperatures on mass and possibly heat transfers within the soil and at the surface in a relatively simple fashion. A temperature-dependent empirical formulation for the reduction of the soil hydraulic conductivity is used by some implicit-ice schemes to increasingly limit vertical soil water fluxes (including infiltration and drainage) as the soil temperature depression (below freezing) increases (Sellers et al. 1996; Boone and Wetzel 1996), or these fluxes are effectively shut off when the corresponding soil temperature falls below freezing (Koster and Suarez 1996). Some implicit schemes [such as Biosphere–Atmosphere Transfer Scheme, or BATS (Dickinson et al. 1993)] allow some effects of latent heating from assumed phase changes.

Explicit schemes typically use a freeze/thaw, drying/wetting analogy to model changes to the soil hydraulic conductivity and matric potential of the soil. Darcy's law can be used to model liquid water transfer in a frozen soil in conjunction with this analogy to a good approximation (Kane and Stein 1983; Spans and Baker 1996). Such schemes can be further characterized in three basic classes. Schemes in the first class consume most or all of the available energy for latent heating, resulting in little to no sensible heating during phase change episodes such that the soil temperature rests at or near the freezing point until all available liquid water has been converted to ice (e.g., Verseghy 1991; Thompson and Pollard 1995; Bonan 1996). Schemes in the second class use simple expressions to parameterize the partitioning of these energies such that sensible heating can be a significant part of the soil energy balance during phase changes (Cogley et al. 1990; Pitman et al. 1991; Slater et al. 1998; Giard and Bazile 2000). A third, slightly more complex class of schemes partitions the available energy based on consideration of an explicit relationship between the soil unfrozen water content and temperature (Cox et al. 1999; Cherkauer and Lettenmaier 1999; Koren et al. 1999). The importance of this distinction with respect to ISBA is examined in a subsequent section of this paper. The scheme described in the current study falls into the second class and is described in the next section.

3. ISBA: Force–restore model

A description of the baseline version of the SVAT scheme called ISBA can be found in NP89 and NM96: only descriptions of the modifications and additions nec-

essary for the inclusion of the two-reservoir soil ice scheme are presented in this paper.

There are seven prognostic equations that describe the exchanges of heat and water among the soil, vegetation, and atmosphere over a column representative of a point or model grid box. Surface soil/vegetation and deep soil (or restore) temperatures, T_s and T_p, a vegetation liquid water interception store, W_r, topsoil and deep soil column volumetric liquid soil water contents, w_s and w_p, and surface and subsurface liquid water equivalent volumetric ice contents, w_{sf} and w_{pf}, respectively, are described by

$$\frac{\partial T_s}{\partial t} = C_T^*[R_n - H - \mathrm{LE}^* - L_f(M_s - \underline{F_{sw}})] - \frac{2\pi}{\tau}(T_s - T_p), \tag{1}$$

$$\frac{\partial T_p}{\partial t} = \frac{1}{\tau}(T_s - T_p) + C_G^* L_f \underline{F_{pw}}, \tag{2}$$

$$\frac{\partial W_r}{\partial t} = \mathrm{veg}P - E_r - R_r \qquad (0 \le W_r \le W_{r\max}), \tag{3}$$

$$\frac{\partial w_s}{\partial t} = \frac{C_1^*}{d_s\rho_w}[(1-\mathrm{veg})P - E_{gl} + R_r + M_s] - \frac{1}{d_s\rho_w}(\underline{F_{sw}} + R_s^*) - \frac{C_2^*}{\tau}(w_s - w_{s\mathrm{eq}}^*) \qquad (w_{\min} \le w_s \le w_{\mathrm{sat}} - w_{sf}), \tag{4}$$

$$\frac{\partial w_p}{\partial t} = \frac{1}{d_p\rho_w}[(1 - \mathrm{veg})P - E_{gl} - E_{tr}^* + R_r + M_s - \underline{F_{pw}} - R_p^*] - \frac{C_3}{\tau}\max(0,\, w_p - w_{fc}^*) \qquad (w_{\min} \le w_p \le w_{\mathrm{sat}} - w_{pf}), \tag{5}$$

$$\frac{\partial w_{sf}}{\partial t} = \frac{1}{d_s\rho_w}(F_{sw} - E_{gf}) \qquad (0 \le w_{sf} \le w_{\mathrm{sat}} - w_{\min}), \tag{6}$$

and

$$\frac{\partial w_{pf}}{\partial t} = \frac{1}{(d_p - d_s)\rho_w}F_{pw} \qquad (0 \le w_{pf} \le w_{\mathrm{sat}} - w_{\min}). \tag{7}$$

A concise description of symbols and the corresponding mks units can be found in appendix C. All of the coefficients and terms that have been directly modified in Eqs. (1)–(5) relative to the model presented by NP89 and NM96 to allow the inclusion of soil ice are denoted using an asterisk (*) superscript, and new variables are underlined. The governing equations for two additional variables relative to the model presented by NM96 are given by Eqs. (6) and (7). Details related to the snow parameterization scheme can be found in Douville et al. (1995).

a. Soil ice evolution

Local changes of the liquid water equivalent volumetric ice content of the soil [Eqs. (6) and (7)] arise solely from soil water phase changes and sublimation of surface-layer soil ice. The phase change terms represent mass fluxes (kg m^{-2} s^{-1}) from either soil ice production or melt, and are expressed for the surface and deep soil layers as

$$F_{sw} = (1 - p_{nc})(F_{sf} - F_{sm}) \quad \text{and} \tag{8a}$$

$$F_{pw} = (1 - p_{nc})(F_{pf} - F_{pm}), \tag{8b}$$

respectively. The first subscript of the phase-change terms (F) represents either the surface (s) or deep-soil (p) layer, and the second one indicates melting (m) or freezing (f). The surface temperature is representative of the uppermost reaches of the combined snow/vegetation layer when the bare-soil portion of the grid box is completely snow covered (i.e., when the soil snow cover fraction, p_{nc}, is unity). The assumed snow depth for total coverage of the bare soil generally is sufficiently large that the restore temperature is also representative of a snow/vegetation layer above or excluding the soil if the snow pack is sufficiently deep. Latent heating/cooling of the soil from phase changes of soil water therefore does not occur in the limit as the surface becomes totally snow covered from Eqs. (8a)–(8b).

The relatively simple so-called energy consumption method for phase change used by ISBA is utilized by other SVAT schemes and most closely resembles those

described by Cogley et al. (1990), Pitman et al. (1991), and Slater et al. (1998). A soil water phase change is modeled to occur if, at the end of a time step, there is available energy and sufficient mass. Ice production from soil water freezing and reduction from melting are parameterized for the surface layer as

$$F_{sf} = (1/\tau_i)\ \min[K_s \epsilon_{sf}\ \max(0,\ T_f - T_s)/C_I L_f,\ \rho_w d_s (w_s - w_{\min})] \quad \text{and} \tag{9a}$$

$$F_{sm} = (1/\tau_i)\ \min[K_s \epsilon_{sm}\ \max(0,\ T_s - T_f)/C_I L_f,\ \rho_w d_s w_{sf}], \tag{9b}$$

and for the deep soil layer as

$$F_{pf} = (\delta_{pf}/\tau_i)\ \min[\epsilon_{pf}\ \max(0,\ T_f - T_p)/C_I L_f,\ \rho_w (d_p - d_s)(w_p - w_{\min})] \quad \text{and} \tag{10a}$$

$$F_{pm} = (1/\tau_i)\ \min[\epsilon_{pm}\ \max(0,\ T_p - T_f)/C_I L_f,\ \rho_w (d_p - d_s) w_{pf}], \tag{10b}$$

where the triple point temperature is represented by T_f (273.16 K), L_f represents the latent heat of fusion of water, and C_I is the ice thermal inertia coefficient [Eq. (B3)]. The liquid equivalent soil ice can fill the soil pore space up to the porosity less a minimum volumetric liquid water content defined as $w_{\min} = 0.01$ ($m^3\ m^{-3}$). The total liquid water content of the soil is simply the sum of the soil water liquid and liquid equivalent ice components.

PHASE CHANGE COEFFICIENTS AND PARAMETERS

The dependency on the insulating effects of the canopy on the surface is modeled in Eqs. (9a)–(9b) as

$$K_s = \left(1 - \frac{\text{veg}}{K_2}\right)\left(1 - \frac{\text{LAI}}{K_3}\right). \tag{11}$$

The dimensionless coefficients related to the vegetation have the values $K_2 = 5.0$ and $K_3 = 30.0$ (Giard and Bazile 2000). The most direct effect of vegetation cover from Eqs. (9a)–(9b) and (11) is to slow the freezing rate of soil water as the vegetation canopy is augmented (i.e., larger values of LAI and veg). This results as energy not used for phase change is assumed to cool/warm the vegetative portion of the lumped soil–vegetation layer. The parameter τ_i (s) in Eqs. (9a)–(10b) represents the characteristic timescale for phase changes, which is related to the rate of freezing in the soil. The value used in this study is 3300 s.

The phase change coefficients, ϵ, introduce a dependence on the water mass available for phase changes and are expressed for the jth soil layer as

$$\epsilon_{jf} = (w_j - w_{\min})/w_{\text{sat}} \qquad (0 \le \epsilon_{jf} < 1) \quad \text{and} \tag{12a}$$

$$\epsilon_{jm} = w_{jf}/(w_{\text{sat}} - w_{\min}) \qquad (0 \le \epsilon_{jm} \le 1), \tag{12b}$$

for soil water freezing and ice melting, respectively. The result of the dependence on soil water content from Eqs. (12a–b) is that a soil layer with a large (small) frozen water fraction can cool (warm) more rapidly than a soil layer with the same thickness and total water content but less soil ice. Soil water freezing ceases from Eq. (12a) when the liquid soil water content value falls below the minimum threshold ($w_{\min}$).

The deep-soil phase change (freezing) term is multiplied by a factor (δ_{pf}) that essentially limits ice production during prolonged cold periods. It is defined as

$$\delta_{pf} = \begin{cases} 1 & z_f < z_{f\max} \\ 0 & z_f \ge z_{f\max}. \end{cases} \tag{13}$$

Ice production can continue up to a maximum threshold defined as $z_{f\max}$, which represents the maximum depth to which the effects of the restore temperature (T_p) extend. It is defined as

$$z_{f\max} = 4/(C_G^* c_g), \tag{14}$$

where C_G^* represents the soil thermal inertia including soil ice (see appendix A for details). The effective depth of soil ice penetration (m) within the soil column is estimated from

$$z_f = d_p\left(\frac{w_{pf}}{w_{pf} + w_p}\right) \qquad (0 \le z_f < d_p). \tag{15}$$

When the effective depth of soil ice exceeds the maximum limit, freezing ceases.

b. Soil water transfer and runoff

The hydrological fluxes and runoff/drainage are evaluated by assuming soil ice becomes part of the solid soil matrix. This is accomplished by defining the modified porosity (e.g., Johnsson and Lundin 1991; Slater et al. 1998) as

$$w_{\text{sat}j}^* = w_{\text{sat}} - w_{fj} \qquad (w_{\min} \le w_{\text{sat}}^* \le w_{\text{sat}}), \tag{16}$$

where w_{sat} is the total soil porosity. The volumetric liquid water content values fall into the range $w_{\min} \le w \le w_{\text{sat}}^*$, where w_{sat}^* represents the maximum holding capacity for liquid water in the soil.

Surface (R_s^*) and total (R_p^*) runoff ($kg\ m^{-2}\ s^{-1}$) results when the corresponding soil layers are saturated. The effective liquid water holding capacity of the soil layers is reduced following Eq. (16) so that runoff can be augmented relative to an ice-free soil subjected to the same combined precipitation and canopy drip rate.

The field capacity (w_{fc}) and wilting point (w_{wilt}) volumetric water contents are defined from the Brooks and Corey (1966) relationships between the soil volumetric water content and the matric potential and hydraulic conductivity with the residual water content parameter set to zero (Clapp and Hornberger 1978). These parameters are modified when soil ice is present using the modified soil porosity from Eq. (16) so that

$$w_{fc}^* = w_{\text{sat}}^*(k_{fc}/k_{\text{sat}})^{1/(2b+3)} = w_{fc}(w_{\text{sat}}^*/w_{\text{sat}}) \quad (0 < w_{fc}^* \le w_{fc}) \quad \text{and} \tag{17a}$$

$$w_{\text{wilt}}^* = w_{\text{sat}}^*(\psi_c/\psi_{\text{sat}})^{-1/b} = w_{\text{wilt}}(w_{\text{sat}}^*/w_{\text{sat}}) \quad (0 < w_{\text{wilt}}^* \le w_{\text{wilt}}), \tag{17b}$$

where critical soil water potential at the permanent wilting point for plants (ψ_c) is defined as -150 m (Mahfouf and Noilhan 1996), and the field capacity is defined following Wetzel and Chang (1987) assuming a hydraulic conductivity (k_{fc}) value of 0.1 mm day^{-1}. The soil saturation matric potential or suction (ψ_{sat}), slope of the soil water retention curve (b), and saturated hydraulic conductivity values (k_{sat}) are defined from Clapp and Hornberger (1978) as a function of soil texture.

Hydraulic conductivity decreases relative to that in a thawed soil as the temperature drops below freezing, most likely because of impedance of liquid flow due to the presence of ice particles (Burt and Williams 1976) and possibly increased viscosity of soil water (Kane and Stein 1983). Drainage [last term in Eq. (5)] is parameterized as a function of hydraulic conductivity in ISBA (Mahfouf and Noilhan 1996), so that it is reduced in accordance with the decrease in liquid soil water holding capacity [Eqs. (16) and (17a)]. The effect of reducing the wilting point [Eq. (17b)] on evaporation is discussed in a subsequent section of this paper.

FORCE–RESTORE COEFFICIENTS

The hydrological force–restore coefficients that control the surface response to water sources/sinks, C_1^*, and vertical diffusion of liquid soil water, C_2^*, and the surface soil water content at the balance of gravity and capillary forces ($w_{s\text{eq}}$) are modified because of the change in the liquid water holding capacity of the soil in the presence of soil ice. The thermal inertia coefficient, C_T^*, is also modified by the presence of soil ice because of changes in the soil thermal inertia (C_G^*). Expressions for the force–restore coefficients can be found in appendix B. The coefficients are plotted as a function of volumetric water content in Fig. 1 for three soil textures using the parameter values from Noilhan and Lacarrère (1995). Solid thick curves are shown for ice-free conditions ($w_{jf} = 0$), and thin curves with opaque symbols represent values using a fixed frozen fraction of 50% ($w_{jf} = w_j$) while varying the total water content (ice and liquid).

The surface hydrological coefficient (C_1^*) increases as the liquid water content of the surface layer (w_s) is transformed into soil ice, which is analogous to drying the soil as water in the liquid phase is reduced (Fig. 1b). In contrast, C_1^* is reduced as the ice fraction in the surface soil layer increases because of a correspondingly smaller value in $C_{1\text{sat}}^*$ [Eq. (B4c)]. Here, C_1^* is plotted as a function of the surface volumetric liquid water content in Fig. 2 for a constant total water content at saturation and at 95% of saturation for three soil textures. For total water content values lower than approximately 90%–95% of saturation, C_1^* is always larger than C_1 for the same total water content when ice is present. The drying effect (increases in C_1^* relative to C_1) dominates except when the total water content is within a few percent of saturation: C_1^* decreases as the frozen fraction increases. This results in a negligible restoring force over the entire range of the freezing fraction in the limit as the surface layer pore space is completely filled.

The primary impact of soil ice on the subsurface soil water vertical diffusion term (C_2^*) is to reduce vertical diffusion (or restore) of liquid soil water from the deep soil into the surface layer. Note that for a sufficiently cold period, w_s can rapidly decrease because of the production of soil ice, whereas changes in w_p occur on a much slower timescale. Because C_2^* and $w_{s\text{eq}}^*$ depend on w_p, an upward liquid soil water flux can be induced from the creation of a liquid soil water gradient, resulting in a net increase in total near-surface soil water. Although this process has been observed (see, e.g., Kane 1980; Kane and Stein 1983; Johnsson and Lundin 1991), it tends to be exaggerated using a diffusion parameterization that depends solely on liquid water content because there is no impedance of fluid flow from augmented surface ice content. Parameterizations assuming a nonlinear dependence on soil ice have been proposed (e.g., Jame and Norum 1980; Johnsson and Lundin 1991) to limit this vertical diffusion, but this introduces an additional model parameter. For simplicity, the C_2^* coefficient is multiplied by a factor that is linearly related to the surface ice [Eq. (B5)]. Using this factor, diffusion decreases in response to an increase in the surface ice fraction and ceases if surface soil ice fills all available pore space. Here, C_2 is plotted as a function of the deep soil layer water content in Fig. 1c assuming that w_{sf} is zero.

The soil thermal inertia, C_G^*, is modified in a manner that is similar to the hydrological coefficients in that the coefficient behaves as if the soil were drying with respect to the deep-soil liquid water content when the fraction of frozen water increases. In addition to this change, C_G^* explicitly includes the heat capacity and thermal conductivity of soil ice. The thermal inertia coefficient is shown as a function of total volumetric water content in Fig. 1a, along with the corresponding thermal inertia value for soil ice, C_I (calculated using the constants defined in Table 1). Even though the thermal inertia of ice is lower than that of the combined soil mineral and water components (C_G) for liquid water content values below approximately field capacity, the drying effect dominates so that the primary effect of soil ice is to augment the soil thermal inertia (C_G^*) relative to the ice-free C_G value for the same total soil water content, except for soils that have rather low total water contents.

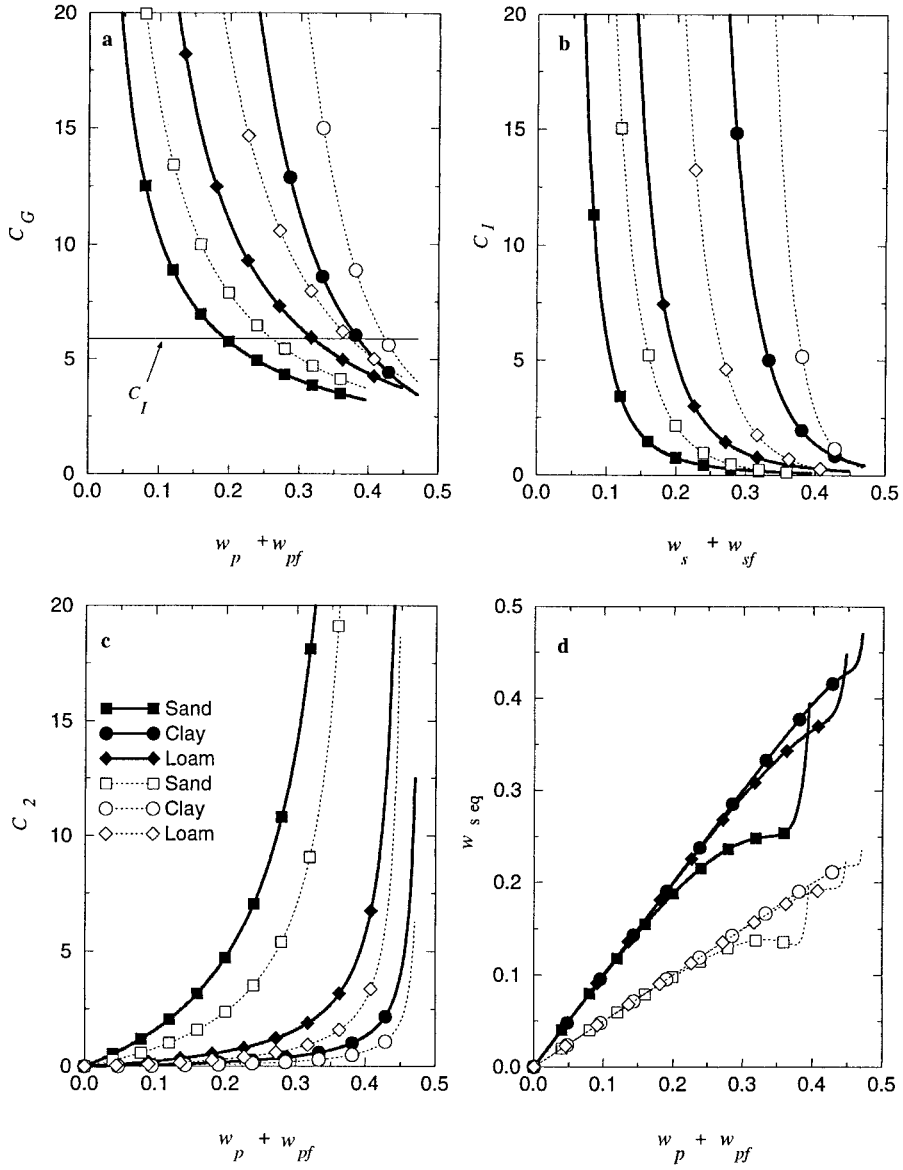

FIG. 1. The soil thermal inertia C_G (10^6 m^2 K J^{-1}), hydrologic force–restore coefficients C_1 and C_2, and the surface volumetric water content at the balance of gravity and capillary forces w_{seq} (m^3 m^{-3}) are shown as a function of total volumetric water content for three soil textures using the Clapp and Hornberger (1978) soil classification scheme. Solid thick curves represent values for ice-free conditions, and the thin curves with opaque symbols represent corresponding values assuming a constant ice fraction of 50% of the total water content. The soil ice thermal inertia coefficient (C_I) is shown in (a).

c. Evapotranspiration

The total latent heat flux (LE*) in Eq. (1) can be expressed as

$$\begin{aligned} \mathrm{LE}^* &= \mathrm{LE}_v^* + \mathrm{LE}_g^* \\ &= L_v(E_r + E_{tr}^* + E_{gl}) + (L_v + L_f)\underline{E_{gf}}, \end{aligned} \quad (18)$$

where L_v and L_f are latent heats of vaporization and fusion, respectively. Evaporation of liquid water intercepted by vegetation, transpiration, and bare-soil evaporation are given by E_r, E_{tr}^*, and E_{gl}, respectively (see NM96 or NP89 for a thorough description of these terms).

Surface resistance in the formulation of transpiration (E_{tr}) is proportional to the soil water stress term, which is written as a function of root-zone layer soil moisture as

$$\theta_p^* = \frac{w_p - w_{\mathrm{wilt}p}^*}{(w_{fcp}^* - w_{\mathrm{wilt}p}^*)} \qquad (0 \le \theta_p^* \le 1). \quad (19)$$

The factor θ_p^* is applied to the stomatal resistance for both the Jarvis (NP89) and the physiological stomatal

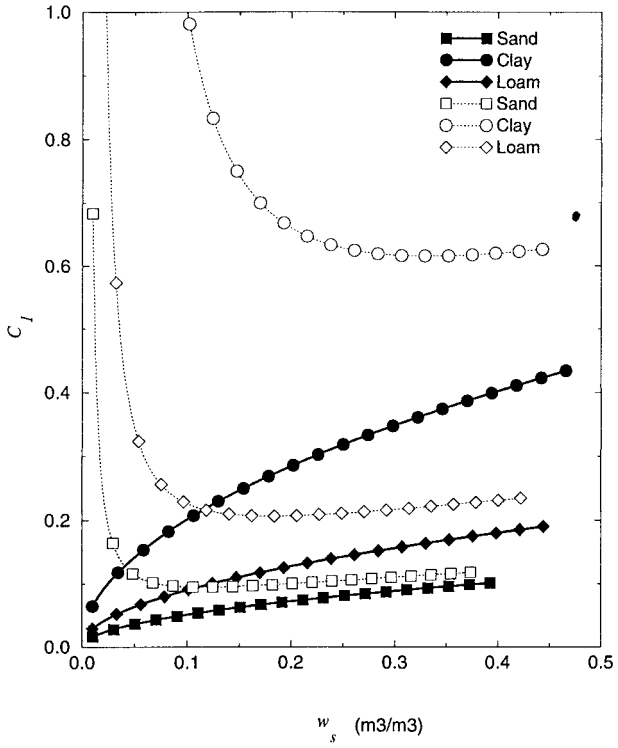

FIG. 2. The hydrologic force–restore coefficient C_1 as a function of the surface soil volumetric liquid water content, w_s, assuming a constant total soil water content at saturation (thick solid curves) and at 95% of saturation (thin dotted curves with opaque symbols) for three soil textures. The volumetric ice content (w_{sf}) decreases as the liquid content increases.

resistance or so-called A-gs methods (Calvet et al. 1998) employed by ISBA. This factor decreases with the inclusion of soil ice, which causes a decrease in transpiration.

Sublimation of soil ice (E_{gf}) is a new term with respect to the ISBA baseline scheme, and it is expressed as

$$E_{gf} = [w_{gf}/(w_{gf} + w_g)](1 - p_{nc})(1 - \text{veg}) \times \rho_a C_H V_a [h_u q_{\text{sat}}(T_s) - q_a]. \quad (20)$$

The first term on the right-hand side of Eq. (20) represents the surface layer soil ice fraction. The sublimation is simply evaluated using the lumped humidity (h_u) over the frozen and ice-free portions of the surface.

4. ISBA-DF: Explicit multilayer model

A relatively high-resolution explicit soil model based on the parameterizations of Philip and de Vries (1957) and de Vries (1958) is coupled to the ISBA surface/vegetation parameterization schemes resulting in the so-called ISBA-DF (ISBA-explicit vertical diffusion) model. In order to facilitate the comparison with ISBA-FR, many simplifying assumptions were made with respect to ISBA-DF. The heat and water transfers are decoupled:

TABLE 1. Physical constants used in ISBA for soil ice.

Symbol	Units (mks)	Value	Description
c_i	J kg^{-1} K^{-1}	2106	Ice specific heat
ρ_i	kg m^{-3}	900	Ice density
λ_i	W m^{-1} K^{-1}	2.22	Ice thermal conductivity

heat transfer is solely along the thermal gradient, while water transfer is induced by gradients in total hydraulic potential (or head). Only the vertical component of the transfer equations is considered. Such assumptions are rather standard of SVAT schemes that use multilayer (defined here as four or more) approaches for climate modeling (e.g., Abramopolous et al. 1988; Thompson and Pollard 1995; Bonan 1996; Cox et al. 1999), mesoscale modeling (e.g., Avissar and Pielke 1989; Wetzel and Boone 1995), or operational numerical weather prediction (e.g., Viterbo and Beljaars 1995; Chen et al. 1996). In essence, ISBA-DF represents the explicit or nonforce–restore version of ISBA because all of the underlying assumptions used to calibrate the heat and mass transfer force–restore coefficients are retained in ISBA-DF.

Governing equations

The governing equations for the heat and mass transfer at the surface and within the soil for ISBA-DF for N soil layers are written as

$$c_s \frac{\partial T_s}{\partial t} = R_n - H - \text{LE} - G_0, \quad (21)$$

$$\Delta z_j c_{gj} \frac{\partial T_j}{\partial t} = G_{j-1} - G_j + L_f F_{jw}, \quad (22)$$

$$\Delta z_j \frac{\partial w_{Lj}}{\partial t} = F_j - F_{j-1} - \frac{1}{\rho_w}(E_{jtr} + E_{gL} + F_{jw}) \quad (w_{\min} \le w_{Lj} \le w_{\text{sat}}), \quad (23)$$

$$\Delta z_j \frac{\partial w_{Ij}}{\partial t} = \frac{1}{\rho_w}(F_{jw} - E_{gI}) \quad (0 \le w_{Ij} \le w_{\text{sat}} - w_{\min}), \quad (24)$$

where the subscript j represents the soil layer ($j = 1, N$). The largest grid resolution is near the surface in order to resolve better the relatively large vertical gradients of heat and liquid water there (see Fig. 3). The surface energy balance is described by Eq. (21), where c_s represents the effective heat capacity of the surface biomass or litter layer slab (Bhumralkar 1975; Blackadar 1979). Although closely related to the (inverse of the) thermal inertia used by the force–restore method [C_T^{-1} in Eq. (1)], c_s can be viewed as a resistance to changes in surface temperature, thereby representing the ability of the bulk surface medium to transfer heat to or from the atmosphere (McNider et al. 1994). The surface temperature, T_s, is assumed to be constant through

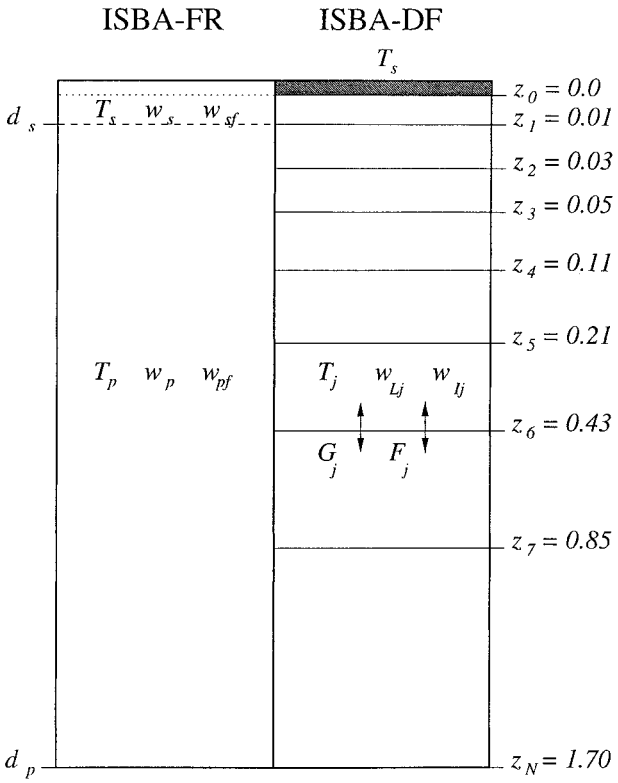

FIG. 3. Schematic diagram of ISBA in force–restore (ISBA-FR: left side) and multiple-layer (ISBA-DF: right side) modes. The soil depths (z) used for the current study are shown on the right side of the diagram in meters. Note that z_0 corresponds to the soil surface. The ISBA-DF soil layer depths are shown on the right side of the diagram (for a total of $N = 8$ layers). Surface (T_s) and soil temperatures (T_p and T), liquid water content (w_s, w_p, and w_L), ice content (w_{sf}, w_{pf}, and w_I), and soil heat (G) and liquid water (F) fluxes are indicated.

this surface layer, and acts as an upper boundary condition for the soil heat flux, G, and a lower boundary condition for calculating the upwelling longwave radiation and surface sensible and latent heat fluxes (Wetzel and Boone 1995). The surface heat fluxes in Eq. (21) are evaluated using the same formulations as in ISBA-FR (NP89; NM96).

The soil heat flux in Eqs. (21)–(22) is written as

$$G = \lambda \frac{\partial T}{\partial z}, \tag{25}$$

where the soil depth, z (m), is increasing downward. The soil thermal conductivity (λ) is expressed as a function of volumetric water content following either the method of Johansen (1975) with modifications by Farouki (1986) as configured for SVAT applications (Peters-Lidard et al. 1998), which explicitly includes the effects of soil ice, or the method of McCumber and Pielke (1981) together with the parameters of Clapp and Hornberger (1978). The latter method is utilized for the current study because it is used implicitly by ISBA-FR with respect to the force–restore coefficients (NP89).

The conservation equations for liquid and liquid equivalent ice volumetric water contents, w_L and w_I, are given by Eqs. (23) and (24), respectively. The vertical soil water flux (m s^{-1}) considering soil water transfers solely arising from pressure gradients is written as

$$F = -k \frac{\partial}{\partial z}(\psi + z) - \frac{D_{v\psi}}{\rho_w} \frac{\partial \psi}{\partial z}, \tag{26}$$

where ψ and k represent the soil matric potential (m) and hydraulic conductivity (m s^{-1}), respectively. The first term on the right-hand side of Eq. (26) represents Darcy's Law for liquid water transfer, and the second term represents a water flux from water vapor transfer. This term is retained in order to be compatible with ISBA-FR, which implicitly includes vapor transfer with respect to the dry soil formulation of the C_1 coefficient. The isothermal vapor conductivity, $D_{v\psi}$, (kg m^{-2} s^{-1}) is a function of soil texture, water content, and temperature following Braud et al. (1993), with some slight modifications for soil ice. For the current study, homogeneous hydraulic properties are assumed for consistency with ISBA-FR.

The soil hydraulic conductivity and matric potential are related to the volumetric liquid water content using the Brooks and Corey (1966) model together with the relationships from Clapp and Hornberger (1978)

$$k = \wp k_{\text{sat}} (w_L / w^*_{\text{sat}})^{2b+3} \quad \text{and} \tag{27a}$$

$$\psi = \psi_{\text{sat}} (w_L / w^*_{\text{sat}})^{-b}, \tag{27b}$$

where the effective porosity, w^*_{sat}, is analogous to the definition used in Eq. (16). The above relationships for matric potential and hydraulic conductivity and the parameter values from Clapp and Hornberger (1978) are used in ISBA-DF because they are implicitly incorporated into ISBA-FR (NP89). The soil parameters, b, ψ_{sat}, and k_{sat} are determined based on the soil texture following Noilhan and Lacarrère (1995). Note that the definition of the hydraulic conductivity is slightly different from the original definition by Clapp and Hornberger through the introduction of the so-called diffusion impedance coefficient $\wp$ (Johnsson and Lundin 1991) defined as

$$\wp = 10^{-a_\wp (w_{Ij}/w_j)},$$

where the value $a_\wp = 6$ is used as proposed by Lundin (1990). It acts to limit vertical soil water fluxes (upward) as a soil layer completely freezes, which is similar to the ice-dependent vertical diffusion impedance factor in ISBA-FR [ISBA-FR C_2 coefficient in Eq. (B5)].

Bare-soil evaporation (E_{gL}) and sublimation (E_{gI}) represent soil water sinks from the uppermost (thin) layer as in ISBA-FR, and transpiration (E_{jtr}) is calculated using the root-zone weighted soil water stress factor (Pan and Mahrt 1987) with modifications for soil ice following Eq. (19). A latent heat source/sink resulting from phase transformation of soil water between the liquid and solid phases is represented by F_{jw}. In the current

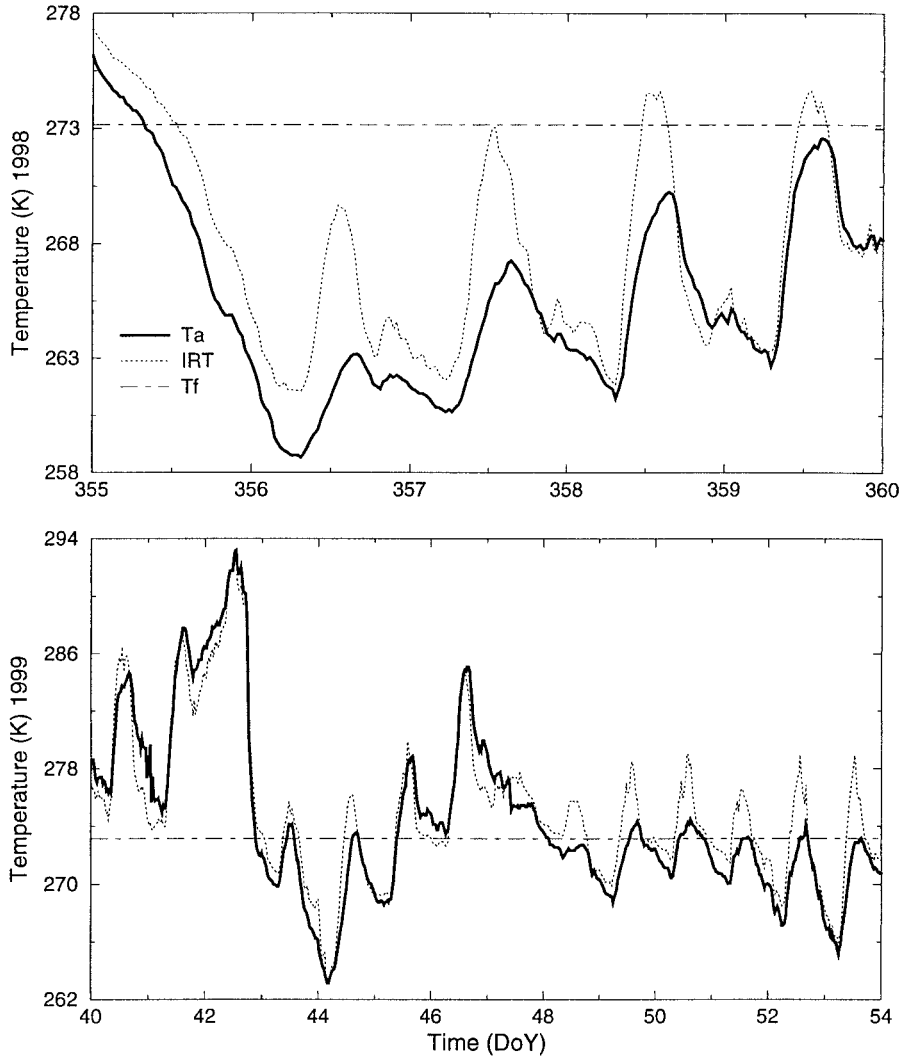

FIG. 4. The observed air (T_a) and surface or skin (IRT) temperatures for the two time periods examined in this study. The solid line represents the air temperature; the dotted line represents the IRT temperature. The dashed line represents the freezing point temperature of water (T_f).

study, it is calculated using any excess energy at the end of the time step analogous to F_{sw} and F_{pw} in ISBA-FR defined by Eqs. (8a)–(8b).

5. Case study

Meyers and Hollinger (1998) describe a dataset gathered from a continental-climate experimental site, which is suited for validation of SVAT schemes. Atmospheric forcing variables (atmospheric temperature, humidity, pressure and wind components, liquid precipitation, and downwelling longwave and shortwave radiation), and surface atmospheric (R_n, H, and LE) and ground heat (G) fluxes are available at 30-min intervals. Temperature observations at soil depths of 0.02, 0.04, 0.08, 0.16, 0.32, and 0.64 m, and volumetric water content at depths of 0.05, 0.20, and 0.60 m are available at a time increment of 30 min. The site is located in Illinois at 40°00.366′N, 88°17.512′W, which is within the Global Energy and Water Cycle Experiment Continental-Scale International Project Large-Scale Area North Central, and on the northeastern edge of the Large-Scale Area Southeast region.

ISBA has been extensively validated in various stand-alone (e.g., Delire et al. 1997; Calvet et al. 1998; Boone et al. 1999) and coupled surface–atmosphere (e.g., Bélair et al. 1998; Giard and Bazile 2000) and macroscale hydrologic (e.g., Habets et al. 1999) model studies (see NM96 for a listing through 1996), so that a full-model validation using the entire Illinois dataset (from 1997–98 and into 1999) is not presented in the current study. The stand-alone version of ISBA driven by prescribed atmospheric forcing without data assimilation is used for the current study. In order to examine the influence

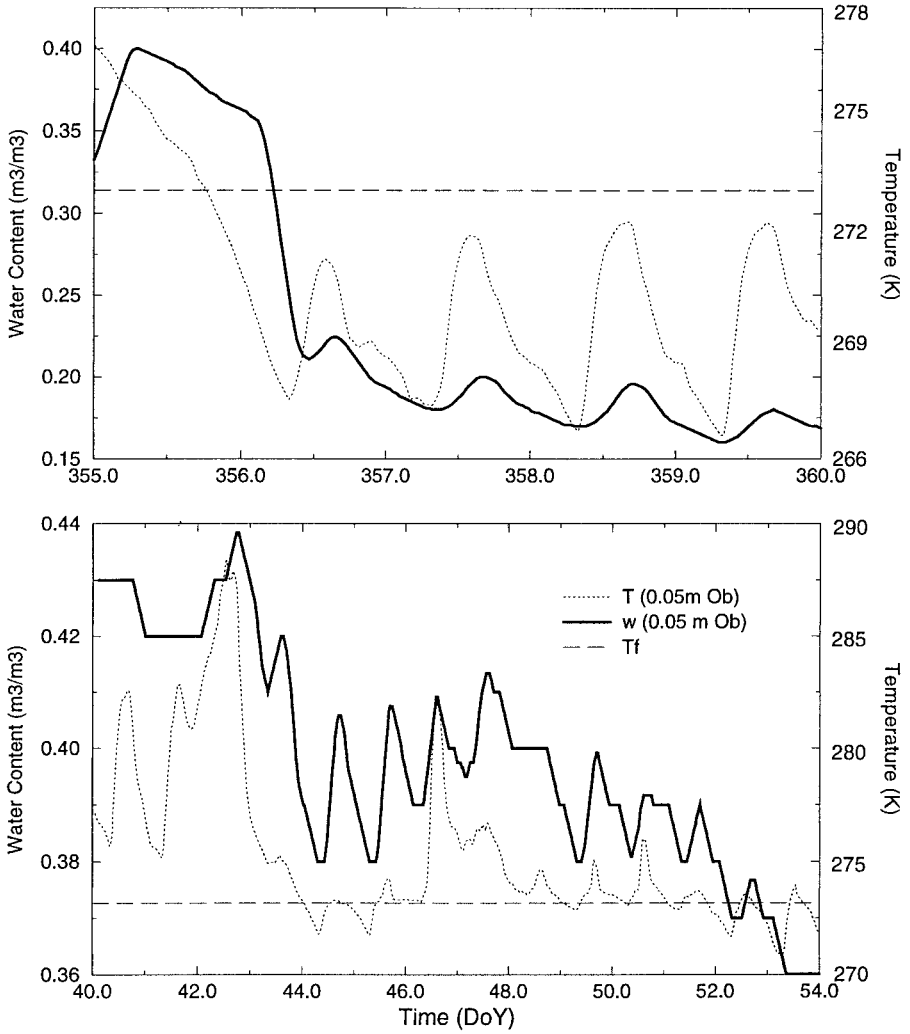

FIG. 5. The observed volumetric water content (w: range indicated along right side of the diagram) and soil temperature (T: range indicated along the left side of the diagram) at a depth of 0.05 m for the two time periods examined in this study. The freezing-point temperature is denoted by T_f. The measured water content decreases when soil ice (not measured) is present.

of soil freezing alone on the model, the periods from day of year (DoY) 355–360, 1998, and DoY 40–54, 1999, were selected for analysis. Air temperatures (T_a) were below freezing for the majority of the time: the period in 1998 encompasses a strong cold outbreak, while the period in 1999 includes a significant freeze thaw cycle followed by several smaller amplitude cycles (see Fig. 4). Periods with little or no snow were selected because the surface properties (albedo, roughness length, insulation, etc.) can change significantly, thereby masking the effects of soil freezing on the surface temperatures and fluxes.

The soil ice content was not measured; however, there is strong evidence of soil ice in the uppermost soil layer. The observed volumetric soil water content and temperature at a soil depth of 0.05 m are shown in Fig. 5 for the two time periods considered. The water content was calculated using the measured dielectric of the soil. Ice has a different dielectric value, and the measured water content values decrease during events when the soil temperature is near or below the freezing point, indicating the presence of soil ice. Furthermore, the magnitudes of the decreases are related to the degree of cooling of the soil. When the observed soil temperatures thawed, the water content returned to nearly the same prefreeze cycle value (not shown), indicating that the total water content changed little during freezing events. Unfortunately, calibration of a relationship between the soil dielectric and ice content for this site is not possible without soil ice measurements. The impact of the inclusion of a soil ice parameterization, therefore, is examined using surface flux and soil temperature data only.

TABLE 2. Baseline parameter values used by ISBA for the Illinois case simulation.

Vegetation parameter	Value (Units)	Soil parameter	Value (Units)
C_v	8.6×10^{-6} (m^2 K J^{-1})	Clay	25.0 (%)
Veg	0.70	Sand	5.0 (%)
Albedo	0.10	τ_i	3300.0 (s)
z_0	0.05 (m)	d_s	0.01 (m)
z_{0h}/z_0	0.1	d_p	1.7 (m)
K_2	5.0	w_{fc}	0.395 (m^3 m^{-3})
K_3	30.0	w_{wilt}	0.186 (m^3 m^{-3})
LAI	0.1 (m^2 m^{-2})	w_{sat}	0.486 (m^3 m^{-3})
Emissivity	1.0	b	6.93
		ψ_{sat}	−0.39 (m)
		k_{sat}	3.11×10^{-6} (m s^{-1})

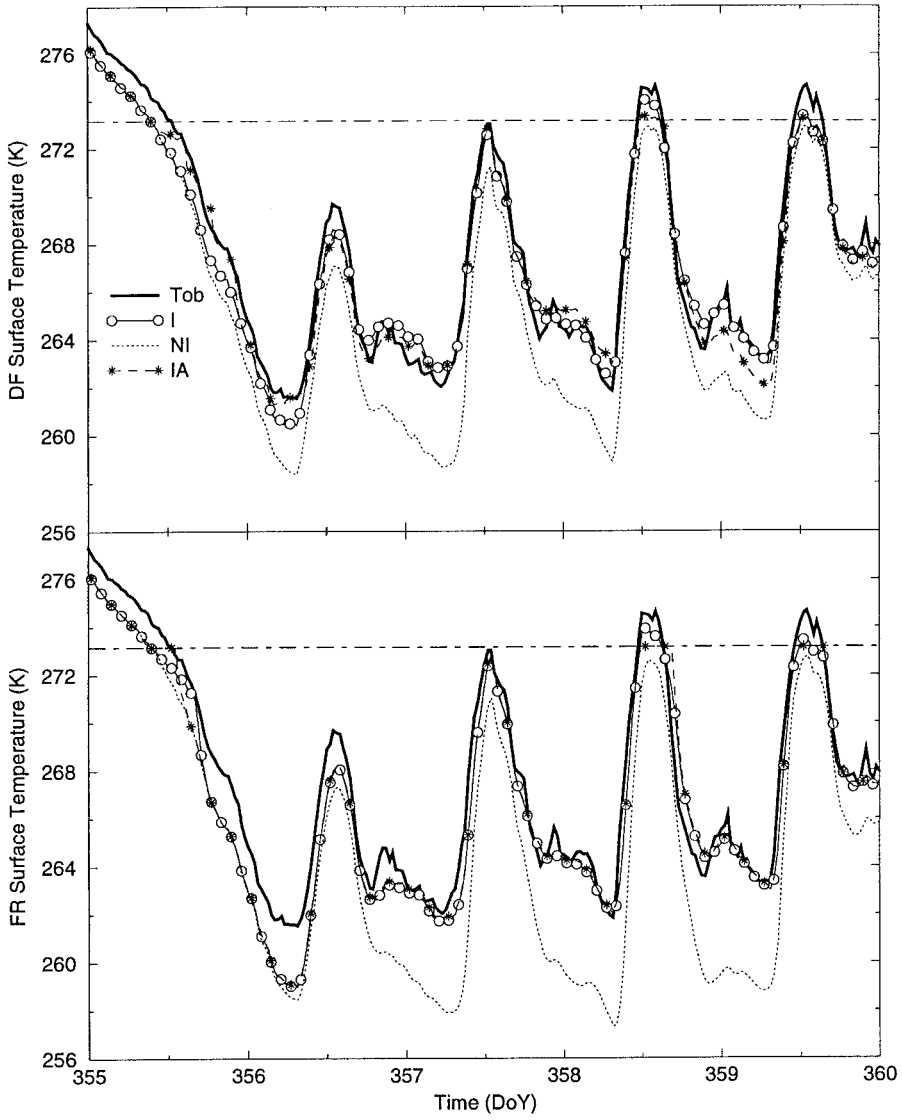

FIG. 6. The observed (thick solid line) and simulated surface temperatures (T_s) for ISBA-DF (top panel) and ISBA-FR (bottom panel). Results from the ice (I), no-ice (NI), and ice using all (IA) available energy for phase transformation tests are represented by the curves that are solid with opaque circles, dotted, and dashed with stars, respectively.

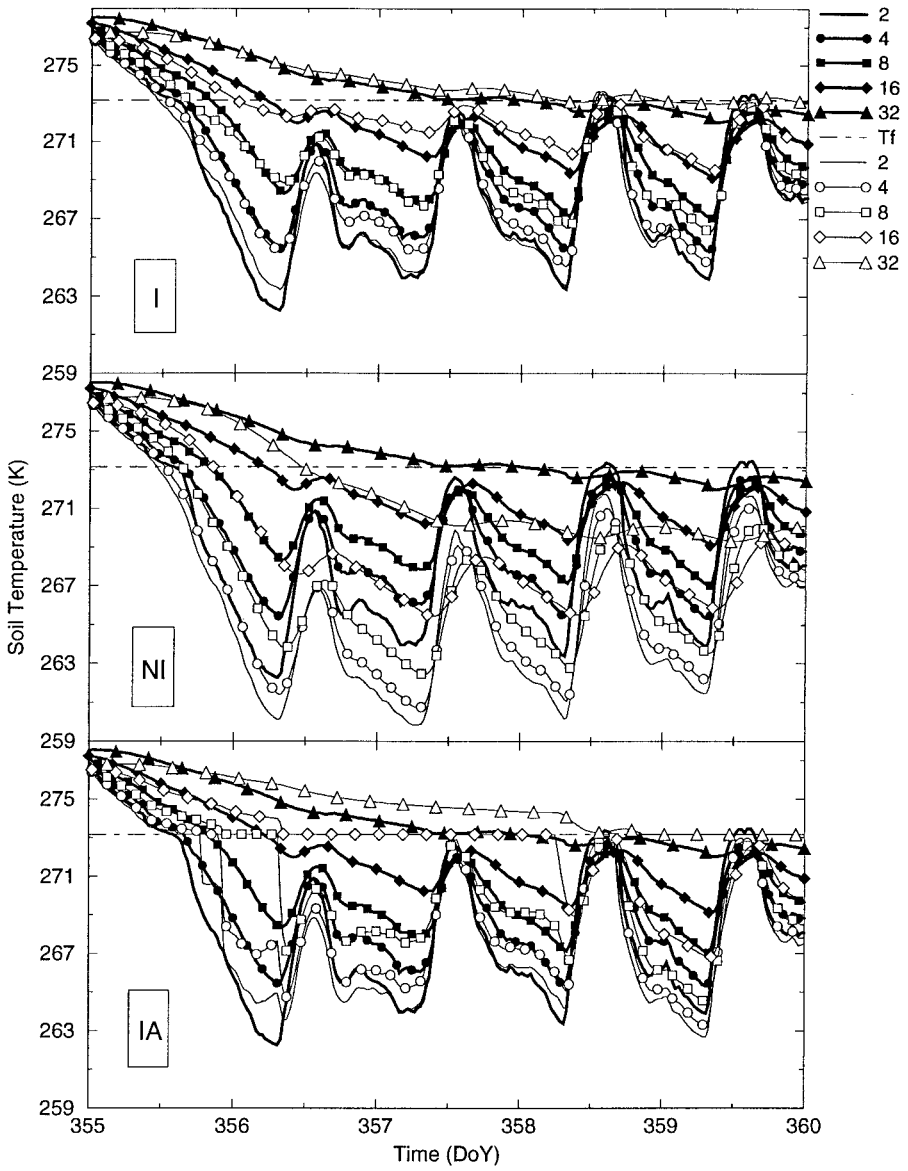

FIG. 7. The modeled (thin lines with opaque symbols) soil temperatures (T_j) for $j = 2, 6$ for the 1998 case. The observed soil temperatures are represented by solid thick lines with filled symbols.

6. Numerical experiments

a. Setup

The first step in the simulation process is to determine appropriate parameters for the vegetation and soil, boundary conditions, model geometry, and initial values for prognostic variables. ISBA was run for one month leading up to the period DoY 355–360, 1998, in order to assure that the soil was ice free, because this period was relatively warm. Numerical tests indicated that this integration time period was more than sufficient to minimize the effects of the initial conditions. An eight-layer soil grid configuration was used for ISBA-DF in order to compare modeled temperatures with the observations at six soil levels (see Fig. 3).

The measured soil textural properties (clay and sand fractions) were used to determine the soil thermal and hydraulic properties following Noilhan and Lacarrère (1995) based on parameter values given by Clapp and Hornberger (1978). The field capacity (w_{fc}) volumetric water content was estimated using the observed profile-mean equilibrium volumetric water content. The soil parameters are listed in Table 2.

No-till agriculture is used at the Illinois site, and the surface consists of bare-soil and a dead-biomass (from a soybean crop in the summer of 1998) layer about

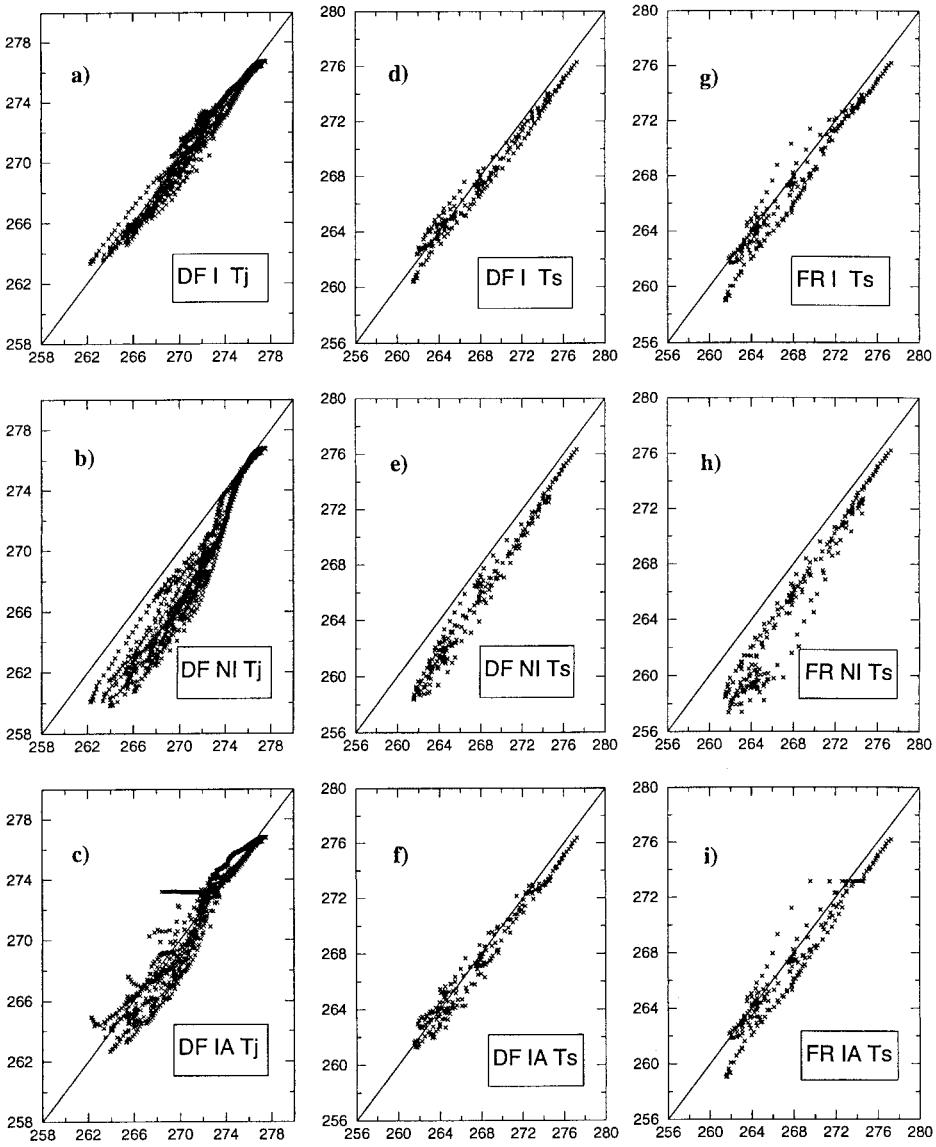

FIG. 8. Relationship between the observed (abscissa) and modeled (ordinate) surface and soil temperatures for the 1998 case. DF corresponds to ISBA-DF (two leftmost columns), while FR corresponds to ISBA-FR (rightmost column). The solid thin line represents a one-to-one relationship. In the leftmost column, soil temperatures for layers 2–6 are plotted together.

0.005 m thick covering the soil. The vegetation parameters used to characterize this site for ISBA are listed in Table 2, and the symbols are defined in appendix C. The only parameter that was not directly available from observations is the vegetation cover fraction (veg). This parameter controls the partitioning of evaporation in ISBA from the nonvegetated (so-called bare soil) and vegetation-covered fractions of the surface (NP89).

The observed soil water content, in general, was at or higher than the soil field capacity (w_{fc}) for the periods considered. This causes modeled bare-soil evaporation to be at the potential rate, which results in latent heat fluxes that were significantly higher than the observed values. It is assumed that the dead-biomass layer is the mechanism responsible for the observed evaporation being below the potential rate because it is known that surface litter can hinder evaporation from the soil (Hillel 1982). The effective ground cover (veg) was then estimated by minimizing the difference between the modeled and observed evaporation during the vegetation-free months prior to the simulation periods in late autumn and early winter of 1998 (when soil water was recharged: that is, at or near field capacity).

TABLE 3. Statistics for DoY 355–360, 1998. Values in parentheses correspond to ISBA-FR: the other values correspond to ISBA-DF. Model variables are shown in the leftmost column. Symbols in the second column correspond to the simulations (defined in the text). Rms errors and biases are in watts per meter squared for the fluxes and kelvins for the temperatures.

		Slope	Intercept	Rms error	R^2	Mean bias
T_1	I	0.98	5.94	1.06	0.97	−0.63
T_s	I	0.91 (1.01)	24.81 (2.63)	0.85 (1.22)	0.98 (0.96)	−0.43 (−0.83)
R_n	I	0.99 (0.99)	0.50 (2.20)	3.47 (4.52)	0.99 (0.99)	0.57 (2.29)
H	I	0.99 (0.90)	19.73 (10.10)	35.91 (25.09)	0.74 (0.89)	19.28 (0.80)
LE	I	1.08 (1.09)	8.30 (9.66)	15.71 (18.02)	0.84 (0.80)	9.63 (11.10)
$\underline{G}$	I	1.12 (1.35)	−13.24 (−11.15)	23.47 (28.15)	0.75 (0.84)	−17.29 (−22.90)
$\overline{F}$	I			19.64 (18.94)		
T_1	NI	1.10	−29.81	1.55	0.97	−1.01
T_s	NI	1.12 (1.20)	−35.31 (−57.06)	2.40 (3.37)	0.98 (0.95)	−2.23 (−3.03)
R_n	NI	0.97 (0.97)	7.70 (11.00)	8.96 (12.99)	0.99 (0.99)	7.93 (11.26)
H	NI	0.79 (0.78)	−7.89 (−12.53)	28.25 (35.51)	0.78 (0.82)	−14.21 (0.68)
LE	NI	0.91 (0.85)	4.60 (2.65)	12.29 (13.12)	0.80 (0.75)	3.13 (0.16)
$\underline{G}$	NI	0.98 (1.49)	5.84 (31.96)	15.93 (32.69)	0.72 (0.65)	6.37 (15.36)
$\overline{F}$	I			16.36 (23.58)		
T_1	IA	0.95	12.61	1.37	0.94	−0.57
T_s	IA	0.92 (0.98)	20.00 (5.06)	0.86 (1.26)	0.97 (0.95)	−0.41 (−0.76)
R_n	IA	0.99 (1.01)	0.61 (3.22)	3.19 (5.26)	0.99 (0.99)	0.64 (3.12)
H	IA	0.99 (0.89)	24.93 (12.77)	49.82 (28.20)	0.76 (0.76)	0.58 (9.47)
LE	IA	1.02 (1.07)	10.83 (10.14)	20.26 (18.21)	0.71 (0.79)	11.21 (11.22)
$\underline{G}$	IA	1.51 (1.40)	−6.53 (−11.74)	36.03 (30.81)	0.70 (0.83)	−24.02 (−25.15)
$\overline{F}$	IA			27.32 (20.62)		

b. Soil temperatures and surface fluxes

Simulation results are presented first for 1998, then for 1999, for several different experiments. Those that include the ISBA default soil ice physics scheme are indicated using ice (I) and no-ice (NI) refers to the simulations using the original baseline model. An additional set of tests were performed in which it was assumed (consistent with many SVAT models) that all available energy is used for soil water phase changes or latent heating (i.e., $K_s = 1$, $\epsilon = 1$, and $\tau_i = \Delta t$): they are referred to as the ice-all (IA) energy simulations.

Standard statistical measures are used in the following section to evaluate and compare the simulations. The uncertainty in the measurements of net radiation, latent, and sensible heat flux from sensor calibrations is not larger than 10% of the mean flux. The uncertainty in the estimate of the mean fluxes is denoted as that resulting from the natural geophysical variability of physical and biological processes, which is generally accepted to be on the order of approximately 15%.

1) 1998

The observed and simulated surface temperatures (T_s) for both ISBA-FR and ISBA-DF are shown in Fig. 6. The surface temperature is simulated with reasonable accuracy for both ISBA-FR and ISBA-DF when soil ice is included (I). The ISBA-FR I simulation is as good as that of ISBA-DF, which can be considered as a reference, except for the first day (DoY 355). In contrast, the NI surface temperature is far too cold from DoY 356–359 for both models. This primarily results from the lack of latent heat release within the soil from soil water freezing. This deficiency is illustrated in more detail in Fig. 7 using ISBA-DF, where filled symbols represent the observed temperatures, and opaque symbols correspond to the model. The modeled temperatures (T_j, $j = 2, 6$) for the NI simulation fall very rapidly because of the lack of latent heating. The soil is moist so that the thermal conductivity is relatively large, which enhances the rapid penetration of surface cooling. In contrast, for the I case, the wet nature of the soil acts to slow the penetration of the freezing front (relative to a drier soil) because there is a large amount of liquid water available for phase change.

The bottom panel in Fig. 7 illustrates basic features of the IA simulation: soil temperatures remain at freezing until all available liquid water has frozen, which is followed by a sudden rapid drop in temperature. This process does not seem to be at work in the soil because the observed transition from thawed to frozen conditions seems to be relatively smooth, especially near the surface (upper 0.08 m of the soil) even though the soil is very moist (see section 5). Deeper within the soil (at a depth of 0.32 m), however, freezing is more gradual so that little energy is going into sensible heating of the soil.

Surface and soil temperature statistics for the I, NI, and IA tests are shown graphically in Fig. 8 and are summarized in Table 3, where ''Intercept'' corresponds to the value of the intercept of a linear fit of the relationship between the observed (abscissa) and modeled (ordinate) values. The root-mean-square (rms) errors are also indicated (K), and R^2 represents the square of the correlation coefficient. The surface temperature is modeled quite well by both the ISBA-FR and ISBA-DF

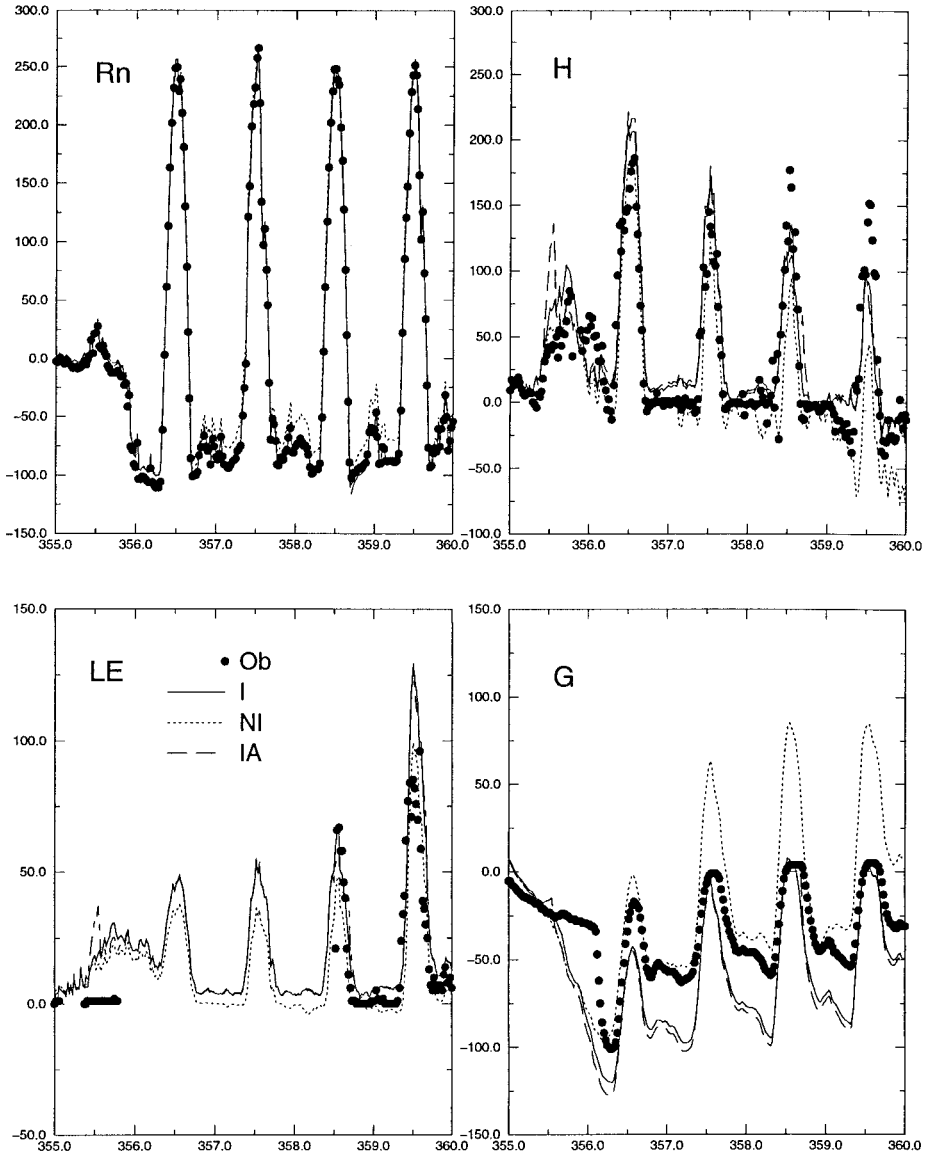

FIG. 9. The net radiation (R_n), sensible (H), latent (LE), and ground (G) heat fluxes (W m^{-2}) from ISBA-FR for 1998. Observations are represented by the filled circles; the I, NI, and IA test simulations are denoted using solid, dotted, and dashed lines, respectively.

models when soil ice is included. Note that even though the I simulation produces the best overall results, there are not significant statistical differences in surface temperature prediction between the I and IA methods for both ISBA-FR and ISBA-DF. This is most likely the case because the surface layer remains frozen for most of this particular simulation period. The subsurface soil temperatures (ISBA-DF only) are best simulated with the I method.

The surface fluxes are shown in Fig. 9 (ISBA-FR) and Fig. 10 (ISBA-DF), and statistics are presented in Table 3, where flux rms errors are in watts per meter squared, and the average rms error for the four surface fluxes is represented by $\overline{F}$. Net radiation (R_n) is modeled quite well for the entire period by both versions of ISBA, especially for the I case. The ground heat flux (G), however, is more problematic. An excessive amount of energy is transferred into the soil via ground heat flux during the daytime for the ISBA-FR NI method (Fig. 9). This results because the deep soil temperature cools far too much during the preceding night, primarily because of the lack of latent heat release within the soil. The large G values during the day cause an underprediction in H and LE from DoY 356–359 inclusive for the NI simulation.

At night, the ISBA-FR NI simulated G compares best with the observed values. This results because the soil transfers too much heat to the surface from below for

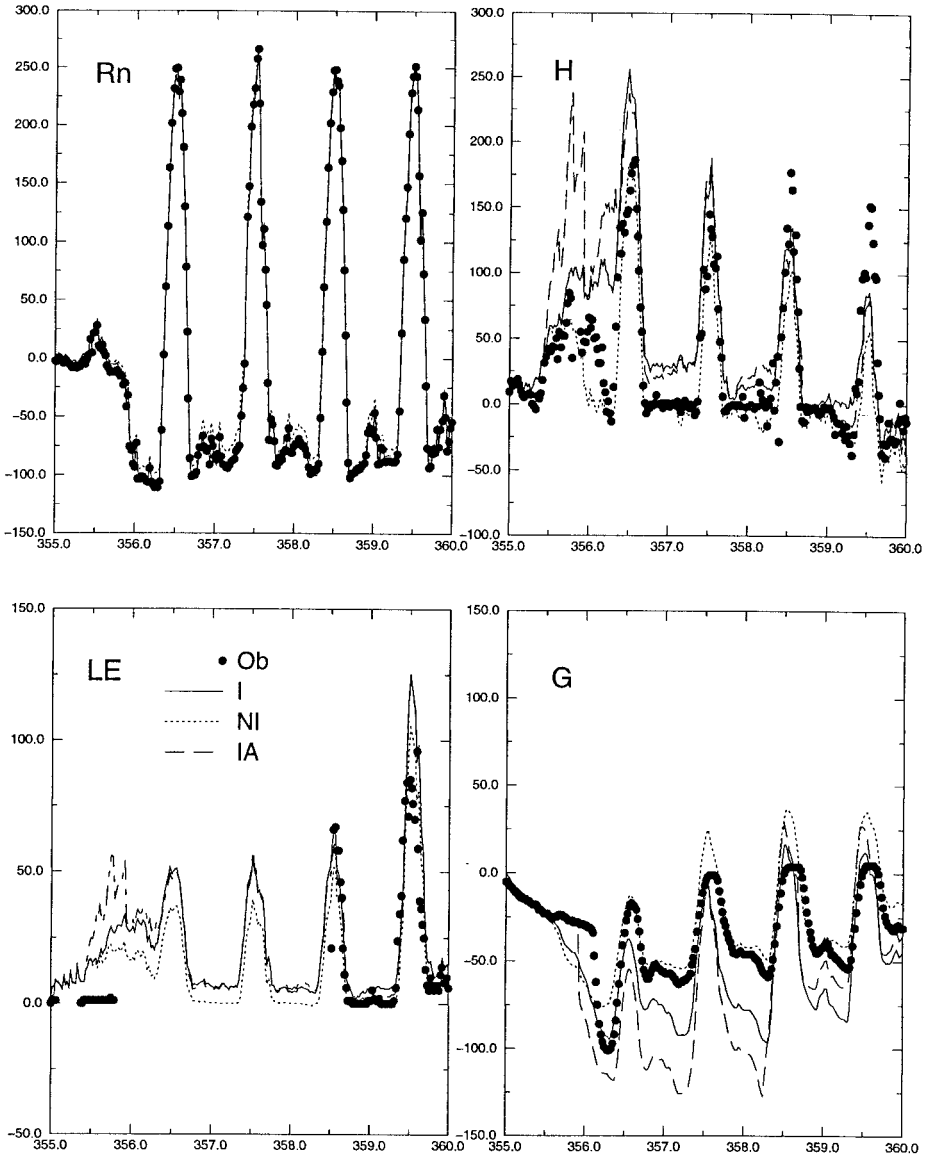

FIG. 10. As in Fig. 9, but for ISBA-DF.

the I and IA simulations. This heat is primarily manifested as positive sensible heat fluxes at the surface. This could be due to the thermal conductivity parameterization, although both methods used by ISBA (NP89 and Johansen 1975) give similar results for this time period. Overall, the lowest ISBA-FR RMS errors for the surface fluxes are obtained for the I simulation (Table 3).

The ground heat flux (G) is better simulated for ISBA-DF, although there are still significant errors primarily at night for the I and IA simulations. DoY 355–356 poses the greatest problems for ISBA-DF with respect to the sensible (H) and latent (LE) heat fluxes (Fig. 10). The ISBA-DF IA surface temperature rests at the freezing point until all of the soil water in the uppermost 0.01 m has frozen, thus causing an erroneously large sensible heat flux. The I simulation also overestimates the sensible heat flux, but to a lesser degree. The NI simulation, on the other hand, underpredicts H because of excessive cooling on DoY 355, but on DoY 356, it produces the best simulation of H. Note that the surface temperature is better modeled by the I and IA cases in comparison with the NI case, which results in a larger surface-to-atmosphere temperature gradient, thereby enhancing the surface heat flux. So, there is a slight inconsistency between the surface temperature and the sensible heat flux for this time period that is difficult to resolve. Also note that for the entire period,

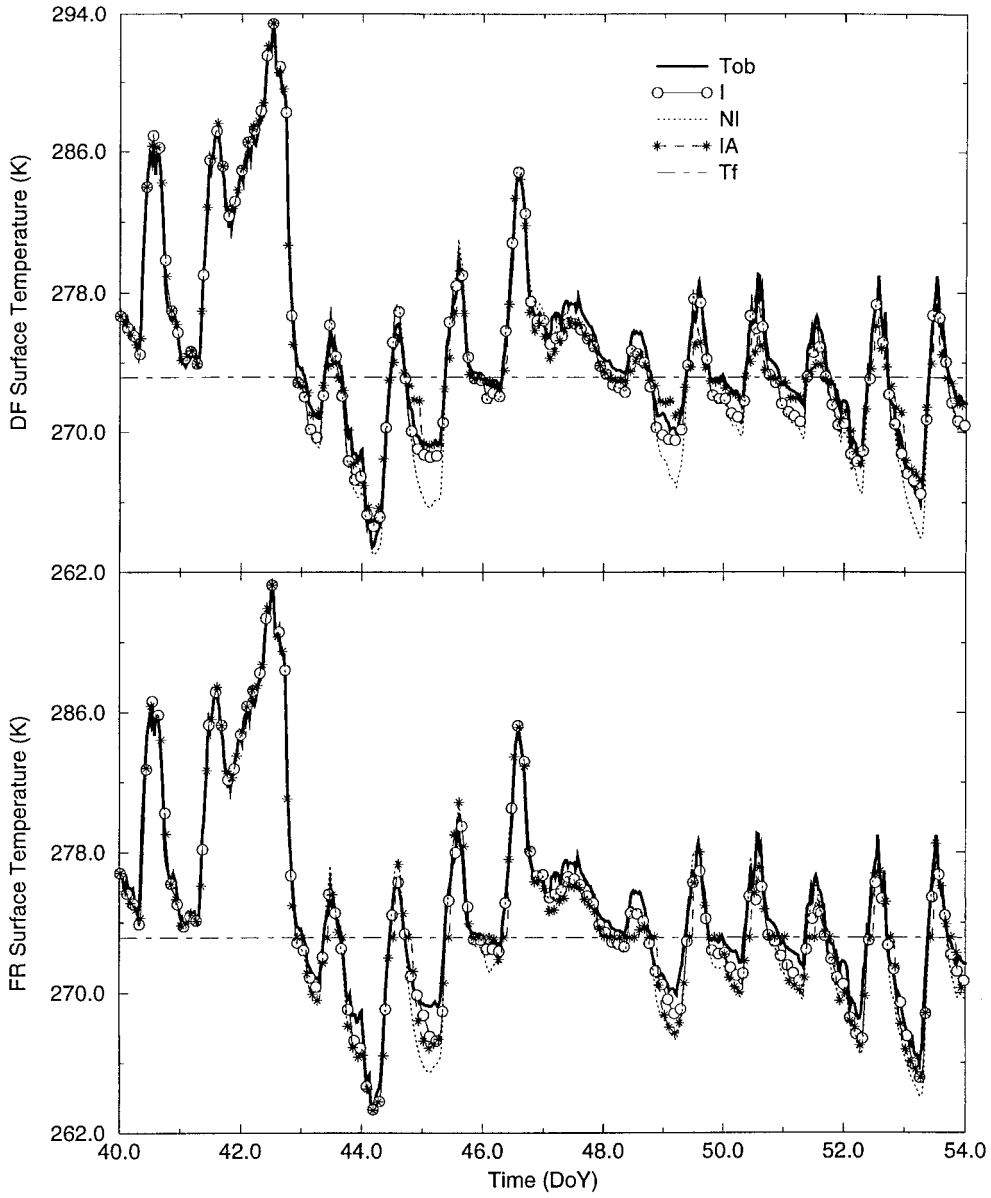

FIG. 11. As in Fig. 6, but for the 1999 case period.

the slope of the linear relationship between the modeled and observed *H* is 0.99 for the I simulation, and 0.79 for the NI simulation.

All versions of ISBA overestimate the latent heat flux on DoY 355. Whether this is a problem with the model or the observations is not known. The observed latent heat flux is nearly zero for a very moist soil for relatively windy and cloudy conditions on DoY 355, so that the observations of LE for this time period are questionable. The overall rms errors in LE and *H* are the lowest for ISBA-DF NI, primarily because of overprediction of the fluxes on DoY 355–356. The ISBA-DF IA flux prediction is the worst overall for the three tests, which is primarily caused by the fact that the soil temperature is constant as the soil layers freeze on DoY 355–356.

2) 1999

The surface temperatures for the period from DoY 40 through DoY 54 are shown in Fig. 11. The ISBA model is able to model the extreme period from DoY 40–44 very well. The ISBA-FR model, however, tends to cool the surface too much on DoY 45 and 49, while only the NI simulation fails in this respect for ISBA-DF. This implies the failure on these two nights by ISBA-FR is possibly related to the resolution difference:

TABLE 4. As in Table 3, but for DoY 40–54, 1999. Rms errors and biases are in watts per meter squared for the fluxes and kelvins for the temperatures.

		Slope	Int.	Rms error	R^2	Mean bias
T_j	I	0.95	13.63	0.98	0.93	−0.23
T_s	I	1.05 (1.06)	14.19 (−17.06)	0.84 (0.94)	0.98 (0.99)	−0.43 (−0.55)
R_n	I	0.99 (0.99)	2.26 (2.62)	3.92 (4.37)	0.99 (0.99)	1.92 (2.53)
H	I	0.99 (0.87)	−5.00 (−5.74)	30.11 (27.81)	0.88 (0.79)	−5.32 (−8.75)
LE	I	0.99 (0.97)	2.24 (2.21)	20.26 (22.43)	0.79 (0.75)	1.91 (1.36)
$\underline{G}$	I	0.91 (1.39)	−3.29 (−0.94)	16.56 (24.80)	0.84 (0.74)	−2.82 (−2.93)
$\overline{F}$	I			17.71 (19.85)		
T_j	NI	1.08	−23.02	1.33	0.91	−0.41
T_s	NI	1.13 (1.12)	−36.75 (−33.75)	1.29 (1.37)	0.98 (0.98)	−0.70 (−0.83)
R_n	NI	0.98 (0.99)	3.69 (4.24)	5.82 (6.22)	0.99 (0.99)	3.09 (3.70)
H	NI	1.01 (1.02)	−10.46 (−12.88)	27.73 (30.80)	0.83 (0.81)	−10.28 (−12.43)
LE	NI	1.02 (1.00)	0.88 (−0.56)	22.13 (22.65)	0.77 (0.76)	1.34 (−0.49)
$\underline{G}$	NI	0.93 (1.38)	−2.11 (3.87)	18.19 (30.05)	0.81 (0.65)	0.65 (1.82)
$\overline{F}$	I			18.47 (22.43)		
T_j	I	0.88	32.38	1.41	0.85	−0.32
T_s	IA	0.98 (1.07)	6.50 (−20.00)	0.97 (1.28)	0.97 (0.97)	−0.30 (−0.68)
R_n	IA	1.01 (1.01)	1.06 (1.06)	4.56 (4.56)	0.99 (0.99)	1.44 (1.44)
H	IA	0.69 (0.69)	3.26 (3.26)	45.62 (45.62)	0.46 (0.46)	−3.08 (−3.81)
LE	IA	0.84 (0.84)	5.22 (5.22)	23.96 (23.96)	0.68 (0.68)	0.24 (0.24)
$\underline{G}$	IA	0.88 (0.88)	−3.21 (−3.21)	15.05 (15.05)	0.73 (0.85)	0.73 (0.73)
$\overline{F}$	IA			22.24 (24.74)		

ISBA-DF has the general tendency to ''feel'' the effects of the underlying surface during phase changes more directly than ISBA-FR (ISBA-DF tends to be slightly warmer during strong cooling events). The temperature statistics are listed in Table 4 and are shown graphically in Fig. 12. The same general trends are observed that were seen in 1998: the surface and soil temperatures were in overall best agreement with the observed values for the I test.

The flux time series data for ISBA-FR and ISBA-DF for the I test are shown in Fig. 13. Overall, the agreement between the model and observations is good, except for G during the nighttime after DoY 42. The observed ground heat flux is relatively flat, while heat is transferred to the surface by the model. Once again, this could possibly be related to the thermal diffusivity parameterizations in the model, and to the simplified parameterization used for heat storage and radiation attenuation of the biomass (Liang et al. 1998; Liang et al. 1999). Organic material in the soil can substantially reduce the thermal conductivity and therefore the ground heat flux (e.g., Gonzalez-Sosa et al. 1999). It is also possible that there are problems with the observed values. The observed soil heat flux was calculated using a heat flux plate at a soil depth of 0.04–0.05 m. Simple calculations using the observed soil water content (which would tend to underestimate G because of the aforementioned soil water decrease caused by freezing) and the observed soil temperatures produce soil heat fluxes at this soil depth with a distinct diurnal cycle (not shown) more closely resembling the larger-amplitude model output values for G. But note that the relative impact of the errors in G on the other flux components is much less for this case (as compared with the 1998 simulation).

The rms error differences were the lowest for the I fluxes (Table 4), although for some flux components the error differences between the I and NI tests are rather small for both ISBA-FR and ISBA-DF. In contrast, the IA fluxes were much worse, especially with respect to the slope of the linear-fit relationship (0.69 for H) and the correlation coefficient ($R^2 = 0.46$ for H) for the two versions of ISBA. An illustration of this problem in more detail can be seen in Fig. 14. The H and LE values for DoY 50–54 are shown for the I and IA cases for both versions of ISBA. The problem with assuming a constant temperature at the freezing point during freezing or thawing is especially pronounced for ISBA-DF; the surface is too warm at night resulting in overprediction in these two fluxes; the opposite is true during the day when the surface temperatures tend to be too cool (Fig. 11). For an NWP or mesoscale model, for which resolution of the diurnal cycle is important, such differences in predicted fluxes arising from rapid freeze–thaw cycles could be significant.

c. Parameter sensitivity

The value of the ISBA-FR surface layer soil depth, d_s, has a significant impact on T_s because of surface soil ice production/melting. This, in turn, affects the surface energy budget, especially on diurnal timescales. This parameter is implicit in the baseline version of ISBA-FR; it is generally accepted to range from 0.01 to possibly as much as 0.10 m. This depth represents the max-

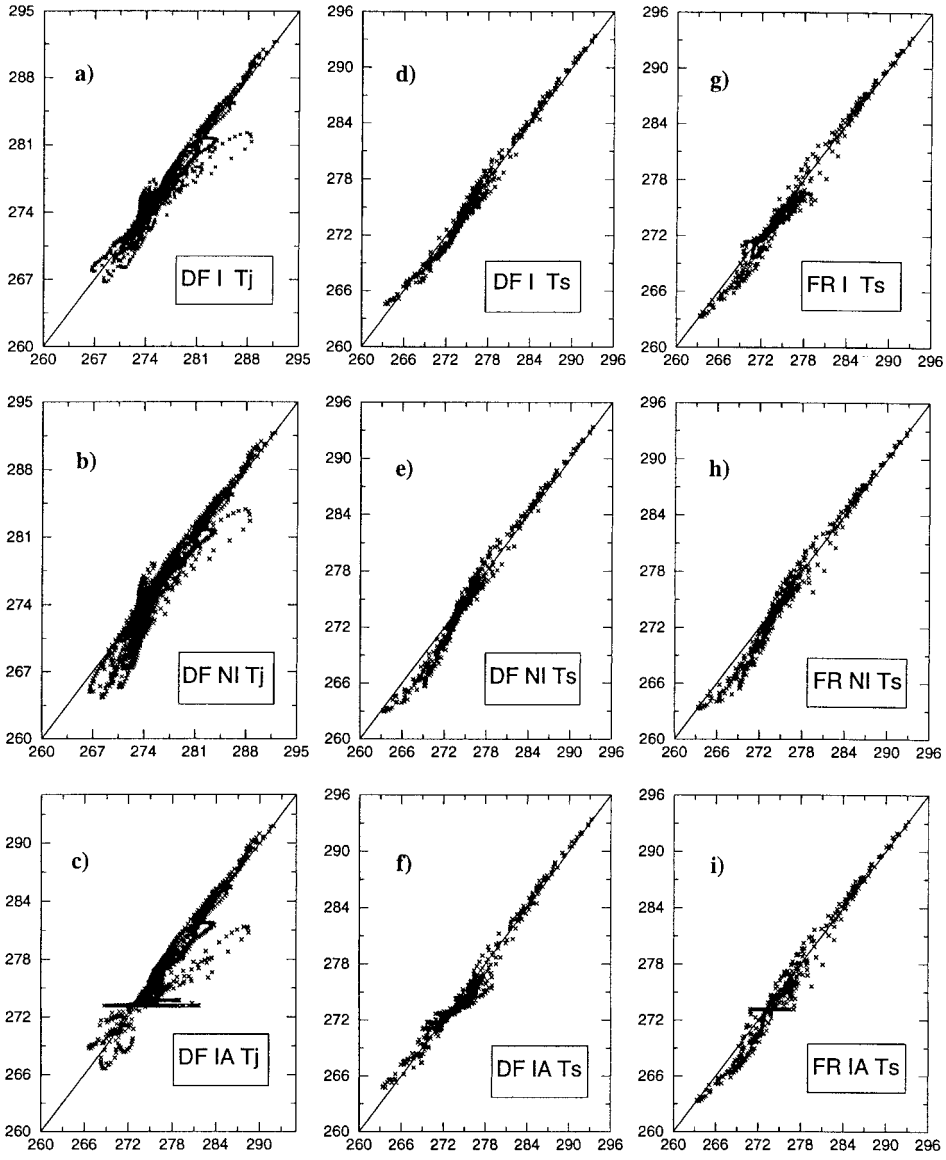

FIG. 12. As in Fig. 8, but for the 1999 case period.

imum depth of the surface ice reservoir in the modified version of ISBA, so that it must be explicitly defined.

In order to examine the impact of the prescribed values of d_s on the model surface temperature and fluxes, the effect of changing the parameter value on rms errors of T_s and $\overline{F}$ were examined. In Fig. 15, results of some simple tests using the 1999 case study are shown. This simulation was selected because many freeze–thaw cycles occur and the time record is longer than that of the 1998 case. The rms errors for the NI cases are plotted along the y axis of the diagrams. The fluxes are best (lowest overall rms errors) simulated for d_s values of approximately the default value used in this study of 0.01 m. The best surface temperature estimates are for d_s values of approximately 0.04 m. After further testing, it was decided to assign d_s a value of 0.01 m in favor of more accurate surface fluxes. The main result of this testing is that the surface ice reservoir, which directly affects the surface energy budget, should be on the order of one to at most several centimeters. It is also noted that no matter what value of d_s was used (over its accepted range) for the 1999 case, the ISBA-FR I results were always superior to the NI simulations (Fig. 15).

7. Discussion

Several noteworthy simplifying assumptions are currently used in ISBA with respect to soil freezing processes. The effects of heaving are neglected because there does not seem currently to be a relatively simple

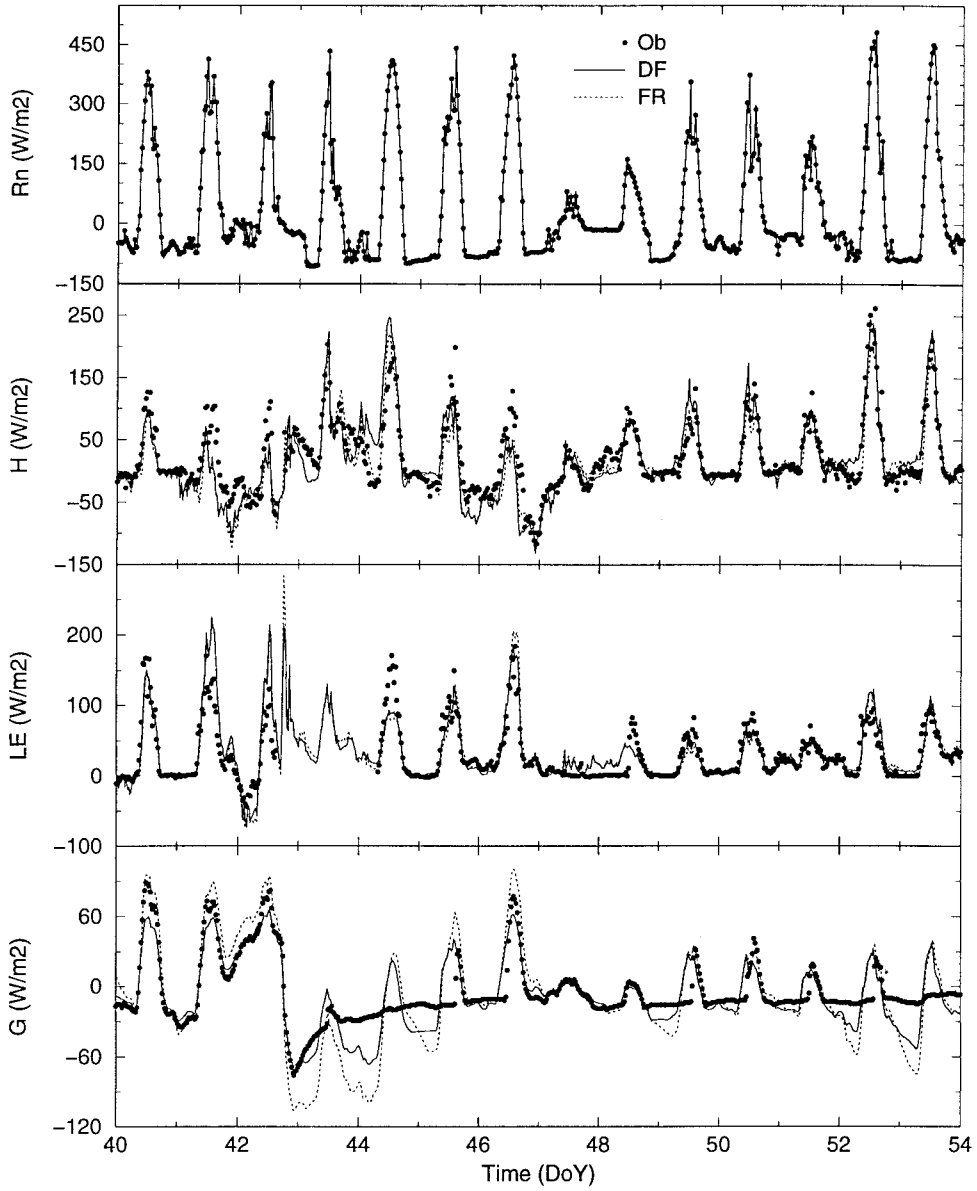

FIG. 13. The net radiation (R_n), and sensible (H), latent (LE), and ground (G) heat fluxes from ISBA-FR (dotted line) and ISBA-DF (solid line) for 1999. Observations are represented by the filled circles.

way to model this process (which is compatible with the force–restore formalism). It can be significant because macropores can develop, which can leave at least temporary routes for rapid water infiltration. Additionally, an explicit relationship between the unfrozen water content and the freezing depression (e.g., Cox et al. 1999; Cherkauer and Lettenmaier 1999; Koren et al. 1999) is not considered in the current study, rather it is modeled using a single parameter, which is more consistent with the relatively simple force–restore approach.

The systematic tuning of many model soil and vegetation parameters was avoided; rather parameters typical of such a site were used when possible. The single variable ice-model parameter (τ_i) is currently constant, but it is suggested that it could eventually be made a function of soil texture in a manner consistent with the other ISBA soil parameters. The single-tuned parameter (veg) was calibrated in late autumn and early winter outside of periods with soil ice and revealed that consideration should be made of the effects of a dead-biomass cover with respect to its ability to suppress evaporation from the soil. This is an important aspect of surface modeling, because some SVAT schemes use a functional dependence between LAI and vegetation-cover fraction.

The use of a single case study site is presented in this

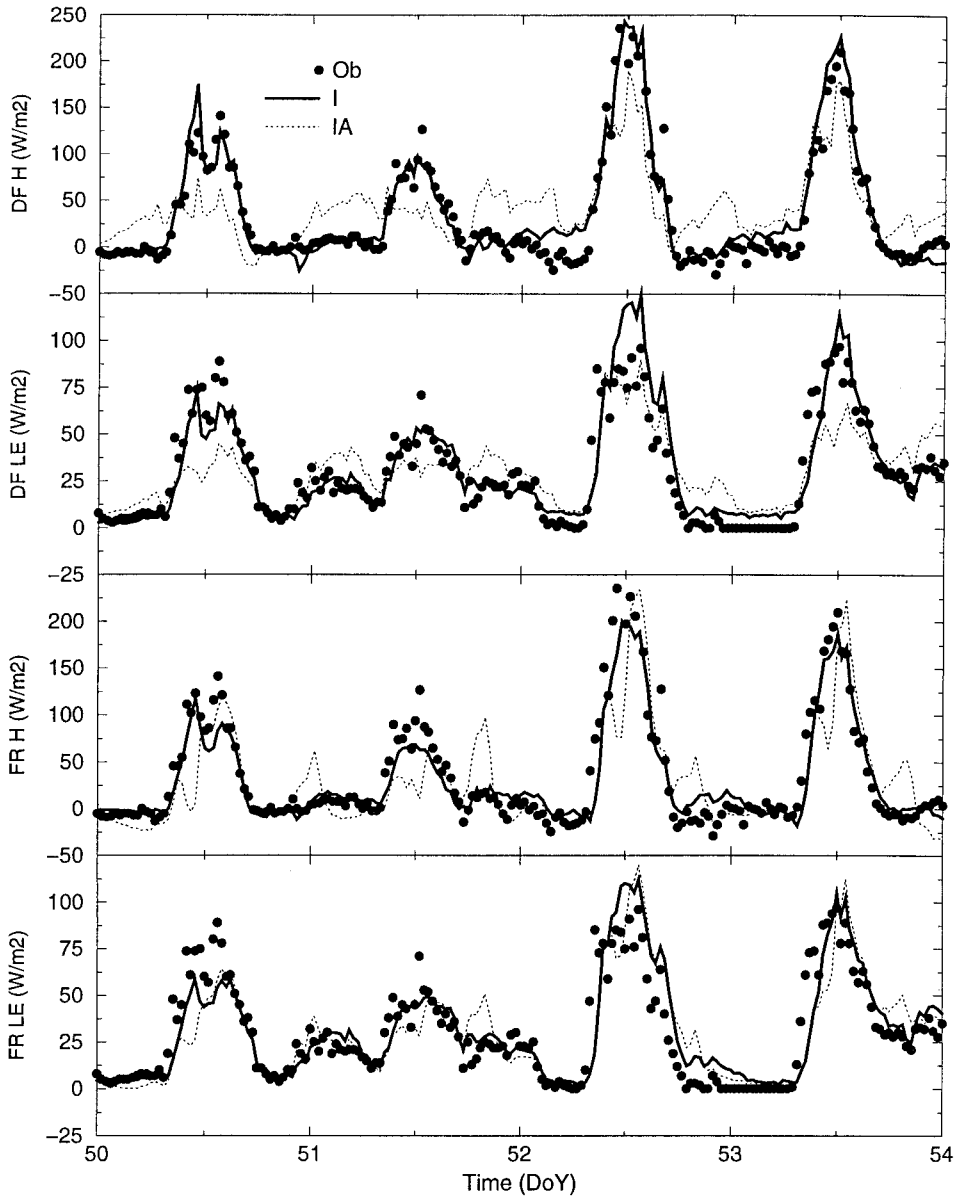

FIG. 14. The sensible (H) and latent (LE) heat fluxes for 1999 for the 4-day period from DoY 50–53, inclusive. Observations are represented by the filled circles. The solid line represents the ISBA simulation with ice (I); the dotted line represents the simulation with ice using all energy available for phase change (IA). ISBA-DF results are in the two uppermost panels; ISBA-FR results are in the lower two panels.

paper; obviously, though, testing must be extended to areas characterized by different soils, vegetative covers, and climates. This will be done as new datasets become available. Because of the lack of soil ice observations, little can be said about the prediction of the actual quantity of soil ice predicted by ISBA-DF and ISBA-FR. The impacts of ice on infiltration and drainage are key aspects that are to be explored in ongoing studies, especially because modeling of soil freezing processes will likely be extended to the version of ISBA that is coupled to the ARPEGE climate model. These aspects, however, are most important in the presence of a snow cover (during ablation in particular): periods with snow cover were avoided for the current study in order to isolate the effects of soil freezing on surface temperature and flux predictions.

It is difficult to extrapolate how the model will behave when feedbacks are permitted with the atmosphere. However, the off-line ISBA results presented in this study are consistent with the results obtained by Giard and Bazile (2000) using ISBA coupled to the ARPEGE NWP model in that nighttime surface temperatures are significantly warmer, including soil freezing from soil water phase-change latent heat release. This helped to

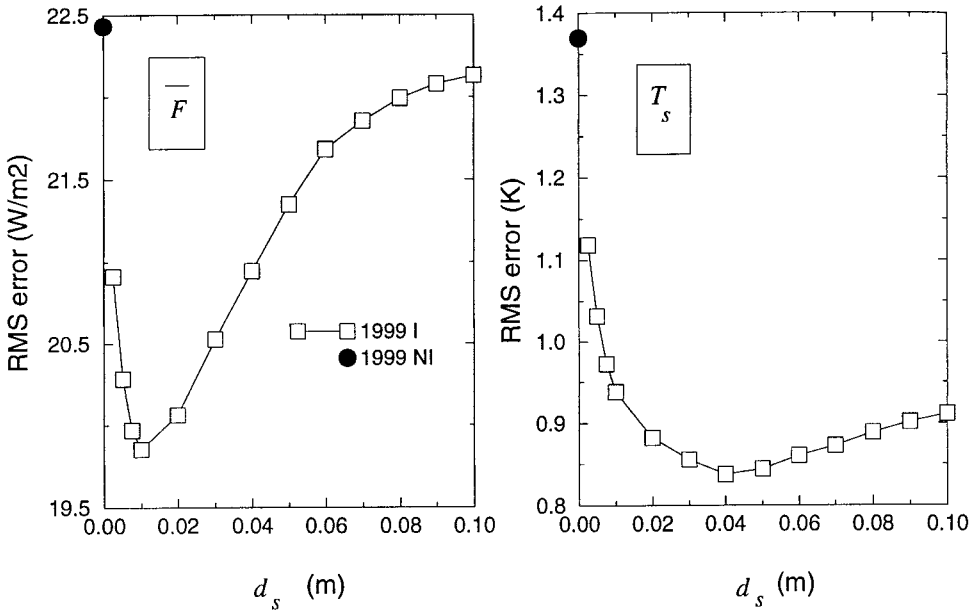

FIG. 15. Sensitivity of simulated surface temperature and average flux rms errors to the values of the ISBA-FR parameter d_s for the 1999 case period. The corresponding rms errors for the NI simulations are plotted using filled circles along the y axis.

diminish a cold bias in predicted temperatures at the lowest atmospheric level in ARPEGE in their study.

An advantage of ISBA-FR relative to ISBA-DF is a computational expense; the explicit multilayer approach nearly doubled the time required for the simulations presented in the current study. It should be noted that the main reason for the increased expense was the relatively large number of layers (SVAT models used for atmospheric applications generally use approximately half the number of layers used in the current study). The computational cost of adding soil ice to the ISBA model was minimal because of the relatively simple formulation used. Possible difficulties with respect to simulating soil-freezing processes by ISBA-FR as compared with ISBA-DF are related to infiltration/surface runoff and ground heat flux. Features captured by a multilayer approach, such as suspended drainage or suppression of infiltration caused by a thin layer of ice near the surface, cannot be explicitly modeled by ISBA-FR.

8. Conclusions

The ISBA SVAT scheme is able to capture the basic features of freeze–thaw cycles and generally produce improved simulations for relatively short-term numerical integration periods typical of NWP models (several days to two weeks) using a simple freeze/thaw, drying/wetting analogy. Surface temperatures are predicted better, especially at night and for a strong cold-outbreak case. Surface fluxes were also predicted better overall for ISBA-FR, although for some time periods/conditions individual surface fluxes were predicted worse in comparison with observations than the baseline case with no soil freezing. It was difficult to discern whether some of these problems were related more to the ice parameterization, some other aspect of the model physics (such as the ground flux or thermal conductivity parameterization), the assigned parameters, or the observations. The physical process that has the greatest impact on the model-simulated surface temperatures and fluxes is the warming (cooling) from latent heat release (absorption) during freezing (thawing).

For the timescales considered in this study (diurnal cycles), the method of freezing must be chosen with care: it was found using ISBA that an assumption of 100% efficiency for phase transformation, which is used by some SVAT schemes designed for climate models, resulted in underestimates of daytime sensible and latent heat fluxes and overestimates at night for this particular micrometeorological case. In order to resolve shorter timescales (diurnal) properly, care must be taken with respect to the method used for partitioning of available energy for phase change.

Last, the ISBA-FR (force–restore) model was able to simulate surface temperatures and fluxes reasonably well in comparison with a higher-resolution (eight layers for the current study) explicit soil model coupled to ISBA (ISBA-DF). General trends in surface temperature and flux predictions resulting from soil freezing were similar between the two schemes. It is unclear at the present time to what level of complexity soil mass and heat transfer processes must be modeled for NWP or climate simulations, so the simplified FR approach is currently used. The ISBA-DF model will continue to

be used to test the accuracy of the simplifying assumptions used by ISBA-FR as more datasets become available for testing and validation.

Acknowledgments. The authors are very grateful to Eva Kowalczyk and Eric Bazile for useful discussions regarding aspects of this research. They also wish to thank three anonymous reviewers for comments regarding this manuscript.

APPENDIX A

Soil Ice Maximum Depth

The restore temperature (T_p) represents the daily average temperature of the composite snow–soil–vegetation surface layer, so that the characteristic length scale can be defined as (Dickinson 1988)

$$z_d = \left(\frac{\lambda\tau}{c_g\pi}\right)^{1/2}, \tag{A1}$$

where τ represents a period of one day. Here, T_p is assumed to be representative of the average temperature over the layer extending from the surface down to a depth of

$$z_{\max} = 2z_d. \tag{A2}$$

The analytical expression for the soil thermal inertia coefficient (C_G) in ISBA (NP89) is defined as

$$C_G = 2\left(\frac{\pi}{\lambda c_g \tau}\right)^{1/2}. \tag{A3}$$

The maximum depth to which the influence of T_p can extend is then determined for ISBA by eliminating thermal conductivity between Eqs. (A1) and (A3), and then substituting Eq. (A1) into Eq. (A2) to have

$$z_{\max} = 4/(C_G c_g). \tag{A4}$$

The maximum freezing depth, $z_{f\max}$, is approximated by replacing C_G by C_G^* in Eq. (A4).

APPENDIX B

ISBA-FR Coefficients

The force–restore coefficients are determined based on soil texture defined as the clay and sand percentages (Noilhan and Lacarrère 1995). All modifications to the expressions for the original coefficients (NP89; NM95) are presented in this appendix.

a. Thermal coefficients

The formulation for the soil/vegetation/snow heat capacity C_T^* is (Douville et al. 1995):

$$C_T^* = 1\Bigg/\left[\frac{(1-\text{veg}_a)(1-p_{nc})}{C_G^*} + \frac{(1-\text{veg}_a)p_{nc}}{C_n} + \frac{\text{veg}_a}{C_v}\right], \tag{B1}$$

where C_n, C_v, and C_G^* are the so-called thermal inertia coefficients for snow, vegetation, and soil, respectively. The apparent vegetation cover, veg_a, is estimated from the snow-free vegetation cover fraction as $\text{veg}_a = \text{veg}(1 - p_{nv})$.

The total soil heat capacity thermal inertia coefficient is calculated as

$$C_G^* = (1 - w_{pf})\min\left[C_{G\max}, C_{G\text{sat}}\left(\frac{w_{\text{sat}p}^*}{w_p}\right)^{b/2\ln(10)}\right] + w_{pf}C_I, \tag{B2}$$

where $C_{G\text{sat}}$ is the soil thermal coefficient at saturation, $C_{G\max}$ is the value at the wilting point water content. The ice heat capacity thermal inertia coefficient is defined as

$$C_I = 2\left(\frac{\pi}{\lambda_i C_i \rho_i \tau}\right)^{1/2}, \tag{B3}$$

where values for the physical constants are listed in Table 1. The total soil thermal inertia is increased as the soil freezes because the liquid water is reduced relative to the total water content, thereby resembling drying. In the limit as the liquid water content falls below the wilting point, however, C_G^* is less than $C_{G\max}$ in the presence of soil ice.

b. Water transfer coefficients

The expression for C_1^* is

$$C_1^* = \begin{cases} C_{1\text{sat}}^*(w_{\text{sat}s}^*/w_s)^{b/2+1} & (w_s \geq w_{\text{wilt}}s^*) \\ f(T_s, w_s, w_{\text{wilt}}^*) & (w_s < w_{\text{wilt}}^*), \end{cases} \tag{B4a}$$

where w_{wilt}^* is defined using the porosity of the surface soil layer in Eq. (17b). The value of C_1 at saturation is expressed (NP89) as

$$C_{1\text{sat}}^* = 2d_s\left(\frac{\pi w_{\text{sat}s}^*}{b|\psi_{\text{sat}}|k_{\text{sat}}\tau}\right)^{1/2}. \tag{B4b}$$

In practice, $C_{1\,\text{sat}}$ is often determined using continuous relationships based on the soil texture (Noilhan and Lacarrère 1995) as opposed to the analytical form above, so that the value for $C_{1\,\text{sat}}$ is scaled as a function of porosity from Eq. (B4b) as

$$C_{1\,\text{sat}}^* = C_{1\,\text{sat}}(w_{\text{sat}s}^*/w_{\text{sat}})^{1/2}. \tag{B4c}$$

The modification of $C_{1\,\text{sat}}$ represents the fact that the soil pore space available for air (volumetric air content) can be limited by the presence of soil ice. This limits vapor diffusion if the soil drying is the result of ice production. Details related to the formulation of C_1 for dry conditions (i.e., when $w_s < w_{\text{wilt}}^*$) can be found in Braud et al. (1993) and Giordani et al. (1996).

The expressions for the surface vertical diffusion restore coefficient (C_2^*) and equilibrium volumetric water content (w_{seq}^*) are written as

$$C_2^* = C_{2\mathrm{ref}}\left(\frac{w_p}{w_{\mathrm{sat}p}^* - w_p + w_l}\right)\left[1 - \left(\frac{w_{sf}}{w_{\mathrm{sat}} - w_{\mathrm{min}}}\right)\right] \quad \text{(B5)}$$

$$\frac{w_{\mathrm{seq}}^*}{w_{\mathrm{sat}p}^*} = \frac{w_p}{w_{\mathrm{sat}p}^*} - a\left\{\left(\frac{w_p}{w_{\mathrm{sat}p}^*}\right)^p\left[1 - \left(\frac{w_p}{w_{\mathrm{sat}p}^*}\right)^{8p}\right]\right\}, \quad \text{(B6)}$$

where a, p, and $C_{2\mathrm{ref}}$ are texture-dependent empirical coefficients (NP89; NM96), and w_l is a small numerical value. The bracketed term in Eq. (B5) is a new factor relative to the formulation of NP89, which has been introduced to limit vertical diffusion (upward) of liquid water into the surface layer as all of the pore space becomes filled with ice.

APPENDIX C

List of Symbols

C_G, C_v	m^2 K J^{-1}	Soil and vegetation thermal inertia coefficients
$C_{G\mathrm{sat}}$	m^2 K J^{-1}	Soil thermal inertia coefficient at saturation
C_H		Drag coefficient
C_I, C_n	m^2 K J^{-1}	Ice and snow thermal inertia coefficients
C_T	m^2 K J^{-1}	Surface thermal inertia coefficient
C_1, C_2, C_3		Force–restore coefficients for soil moisture
$C_{1\mathrm{sat}}$		Value of C_1 at saturation
$C_{2\mathrm{ref}}$		Value of C_2 at 50% saturation
$D_{w\psi}$	kg m^{-2} s^{-1}	Isothermal vapor conductivity
E_{gf}, E_{gl}	kg m^{-2} s^{-1}	Bare-soil sublimation and evaporation
E_r	kg m^{-2} s^{-1}	Evaporation of intercepted water
E_{tr}	kg m^{-2} s^{-1}	Transpiration
F	m s^{-1}	Darcian soil water flux
F_{sw}, F_{pw}	kg m^{-2} s^{-1}	Surface and deep-soil net phase change terms
F_{sf}, F_{sm}	kg m^{-2} s^{-1}	Surface ice freezing and melting
F_{pf}, F_{pm}	kg m^{-2} s^{-1}	Deep-soil ice freezing and melting
H	W m^{-2}	Sensible heat flux
K_s		Surface phase change coefficient
K_2, K_3		Soil water phase change vegetation insulation coefficients
LAI	m^2 m^{-2}	Leaf area index
LE	W m^{-2}	Latent heat flux
L_f, L_v	J kg^{-1}	Latent heats of fusion and vaporization
M_s	kg m^{-2} s^{-1}	Snowmelt flux
P	kg m^{-2} s^{-1}	Precipitation
R_n	W m^{-2}	Net radiative flux
R_s, R_p	kg m^{-2} s^{-1}	Surface and total runoff
R_r	kg m^{-2} s^{-1}	Interception excess/canopy drip
T_f	K	Triple point for water
T_s, T_p	K	Surface and deep-soil (restore) temperatures
V_a	m s^{-1}	Wind speed
W_r	kg m^{-2} s^{-1}	Intercepted water
$W_{r\max}$	kg m^{-2} s^{-1}	Maximum intercepted water
a, p		Coefficients of $w_{s\mathrm{eq}}$ formulation
b		Slope of the soil water retention curve
c_g	J K^{-1} m^{-3}	Soil heat capacity
d_s, d_p	m	Surface and total soil depths
k	m s^{-1}	Soil hydraulic conductivity
k_{fc}	m s^{-1}	Soil hydraulic conductivity at field capacity
k_{sat}	m s^{-1}	Soil hydraulic conductivity at saturation
q_a	kg kg^{-1}	Atmospheric specific humidity
q_{sat}	kg kg^{-1}	Surface saturation specific humidity
veg		Surface vegetation cover fraction
w_{Lj}, w_{Ij}	m^3 m^{-3}	Layer average volumetric water and ice contents
w_{fc}	m^3 m^{-3}	Field capacity volumetric water content
w_s, w_p	m^3 m^{-3}	Surface and total soil volumetric water contents
w_{sf}, w_{pf}	m^3 m^{-3}	Surface and deep-soil water equivalent volumetric ice content
w_{min}	m^3 m^{-3}	Minimum liquid volumetric water content threshold
w_{sat}	m^3 m^{-3}	Soil porosity
w_{sat}^*	m^3 m^{-3}	Saturation value for liquid soil water
$w_{s\mathrm{eq}}$	m^3 m^{-3}	Surface equilibrium/restore water content
w_{wilt}	m^3 m^{-3}	Wilting point volumetric soil water content
z_f	m	Depth of soil ice penetration
$z_{f\max}$	m	Maximum allowable depth of soil ice penetration
z_T	m	Water table depth
z_0	m	Surface roughness length for momentum
z_{0h}	m	Surface roughness length for heat
Δt	s	Model time step
δ_{pf}	ice production	Limit delta function
λ	W m^{-1} K^{-1}	Soil thermal conductivity
ψ	m	Soil water matric potential
ψ_c	m	Critical matric potenial value at wilting point
ψ_{sat}	m	Soil water matric potential at saturation
ρ_a	kg m^{-3}	Lowest atmospheric level air density
ρ_w	kg m^{-3}	Density of liquid water

τ	s	Time constant of one day
τ_i	s	Characteristic timescale for soil water phase change
θ_p		Soil moisture stress coefficient
$\wp$		Liquid water vertical diffusion impedence coefficient

REFERENCES

Abramopoulos, F., C. Rosenzweig, and B. Choudhury, 1988: Improved ground hydrology calculations for global climate models (GCMs): Soil water movement and evapotranspiration. *J. Climate,* **1,** 921–941.

Avissar, R., and R. A. Pielke, 1989: A parameterization of heterogeneous land surfaces for atmospheric numerical models and its impact on regional meteorology. *Mon. Wea. Rev.,* **117,** 2113–2136.

Bélair, S., P. Lacarrère, J. Noilhan, V. Masson, and J. Stein, 1998: High-resolution simulation of surface and turbulent fluxes during HAPEX-MOBILHY. *Mon. Wea. Rev.,* **126,** 2234–2253.

Bhumralkar, C. M., 1975: Numerical experiments on the computation of ground surface temperature in an atmospheric general circulation model. *J. Appl. Meteor.,* **14,** 67–100.

Blackadar, A. K., 1979: High resolution models of the planetary boundary layer. *Adv. Environ. Sci. Eng.,* **1,** 50–85.

Bonan, G. B., 1996: A land surface model (LSM version 1.0) for ecological, hydrological, and atmospheric studies: Technical description and user's guide. NCAR Tech. Note TN-417+STR, 150 pp.

Boone, A., and P. J. Wetzel, 1996: Issues related to low resolution modeling of soil moisture: Experience with the PLACE model. *Global Planet. Change,* **13,** 161–181.

——, J.-C. Calvet, and J. Noilhan, 1999: Inclusion of a third soil layer in a land-surface scheme using the force–restore method. *J. Appl. Meteor.,* **38,** 1611–1630.

Braud, I., J. Noilhan, P. Bessemoulin, P. Mascart, R. Havercamp, and M. Vauclin, 1993: Bareground surface heat and water exchanges under dry conditions: Observations and parameterization. *Bound.-Layer Meteor.,* **66,** 173–200.

Brooks, R. H., and A. T. Corey, 1966: Properties of porous media affecting fluid flow. *J. Irrig. Drain. Amer. Soc. Civ. Eng., IR,* **2,** 61–88.

Burt, T. P., and and P. J. Williams, 1976: Hydraulic conductivity in frozen soils. *Earth Surf. Processes,* **1,** 349–360.

Calvet, J.-C., J. Noilhan, J.-L. Roujean, P. Bessemoulin, M. Cabelguenne, A. Olioso, and J.-P. Wigneron, 1998: An interactive vegetation SVAT model tested against data from six contrasting sites. *Agric. For. Meteor.,* **2564,** 1–23.

Chen, F., and Coauthors, 1996: Modeling of land surface evaporation by four schemes and comparison with FIFE observations. *J. Geophys. Res.,* **101,** 7251–7268.

Cherkauer, K. A., and D. P. Lettenmaier, 1999: Hydrologic effects of frozen soils in the upper Mississippi River basin. *J. Geophys. Res.,* **104,** 19 599–19 610.

Clapp, R., and G. Hornberger, 1978: Empirical equations for some soil hydraulic properties. *Water Resour. Res.,* **14,** 601–604.

Cogley, J. G., A. J. Pitman, and A. Henderson-Sellers, 1990: A land surface for large scale climate models. Tech. Note 90-1, Trent University, Peterborough, ON, Canada, 129 pp.

Courtier, P., and J.-F. Geleyn, 1988: A global numerical weather prediction model with variable resolution. Applications to the shallow water equations. *Quart. J. Roy. Meteor. Soc.,* **114,** 1321–1346.

Cox, P. M., R. A. Betts, C. B. Bunton, R. L. H. Essery, P. R. Rowntree, and J. Smith, 1999: The impact of new land surface physics on the GCM simulation of climate and climate sensitivity. *Climate Dyn.,* **15,** 183–203.

Deardorff, J. W., 1977: A parameterization of ground surface moisture content for use in atmospheric prediction models. *J. Appl. Meteor.,* **16,** 1182–1185.

——, 1978: Efficient prediction of ground surface temperature and moisture, with inclusion of a layer of vegetation. *J. Geophys. Res.,* **83,** 1889–1903.

Delire, C., J.-C. Calvet, J. Noilhan, I. Wright, A. Manzi, and C. Nobre, 1997: Physical properties of Amazonian soils: A modeling study using the Anglo–Brazilian Amazonian climate observation study data. *J. Geophys. Res.,* **102,** 30 119–30 133.

de Vries, D. A., 1958: Simultaneous transfer of heat and moisture in porous media. *Eos, Trans. Amer. Geophys. Union,* **39** (5), 909–916.

Dickinson, R. E., 1984: Modeling evapotranspiration for three-dimensional global climate models. *Climate Processes and Climate Sensitivity, Geophys. Monogr.,* No. 5, Amer. Geophys. Union.

——, 1988: The force-restore model for surface temperatures and its generalizations. *J. Climate,* **1,** 1086–1097.

——, A. Henderson-Sellers, and P. J. Kennedy, 1993: Biosphere–Atmosphere Transfer Scheme (BATS) Version 1e as coupled to the NCAR Community Climate Model. NCAR Tech. Note TN-387+STR, 72 pp.

Douville, H., J. F. Royer, and J.-F. Mahfouf, 1995: A new snow parameterization for the Meteo-France climate model. *Climate Dyn.,* **12,** 21–35.

Farouki, O. T., 1986: *Thermal Properties of Soils.* Series on Rock and Soil Mechanics, Vol. 11, Trans Tech Publications, 136 pp.

Giard, D., and E. Bazile, 2000: Implementation of a new assimilation scheme for soil and surface variables in a global NWP model. *Mon. Wea. Rev.,* **128,** 997–1015.

Giordani, H., J. Noilhan, P. Lacarrère, and P. Bessemoulin, 1996: Modeling the surface processes and the atmospheric boundary layer for semi-arid conditions. *Agric. For. Meteor.,* **80,** 263–287.

Gonzalez-Sosa, E., I. Braud, J.-L. Thony, M. Vauclin, P. Bessemoulin, and J.-C. Calvet, 1999: Modeling heat and water exchanges of fallow land covered with plant-residue mulch. *Agric. For. Meteor.,* **2682,** 1–19.

Habets, F., and Coauthors, 1999: The ISBA surface scheme in a macroscale hydrological model applied to the HAPEX-MOBILHY area. Part 2: Simulation of streamflows and annual water budget. *J. Hydrol.,* **217,** 97–118.

Henderson-Sellers, A., Z.-L. Yang, and R. E. Dickinson, 1993: The Project for Intercomparison of Land-surface Parameterization Schemes. *Bull. Amer. Meteor. Soc.,* **74,** 1335–1349.

——, A. Pitman, P. Love, P. Irannejad, and T. Chen, 1995: The Project for Intercomparison of Land Surface Parameterization Schemes (PILPS): Phases 2 and 3. *Bull Amer. Meteor. Soc.,* **76,** 489–503.

Hillel, D., 1982: *Introduction to Soil Physics.* Academic Press, 364 pp.

Jame, Y.-W., and D. I. Norum, 1980: Heat and mass transfer in a freezing unsaturated porous medium. *Water Resour. Res.,* **16** (4), 811–819.

Johansen, O., 1975: Thermal conductivity of soils. Ph.D. thesis, University of Trondheim, 236 pp. [Available from Universitetsbiblioteket i Trondheim, Høgskoleringen 1, 7034 Trondheim, Norway.]

Johnsson, H., and L.-C. Lundin, 1991: Surface runoff and soil water percolation as affected by snow and soil frost. *J. Hydrol.,* **122,** 141–158.

Kane, D. L., 1980: Snowmelt infiltration into seasonally frozen soils. *Cold Reg. Sci. Technol.,* **3,** 153–161.

——, and J. Stein, 1983: Water movement into seasonally frozen soils. *Water Resour. Res.,* **19,** 1547–1557.

Koren, V., J. Schaake, K. Mitchell, Q.-Y. Duan, F. Chen, and J. M. Baker, 1999: A parameterization of snowpack and frozen ground intended for NCEP weather and climate models. *J. Geophys. Res.,* **104,** 19 569–19 585.

Koster, R. D., and M. J. Suarez, 1996: Energy and water balance calculations in the Mosaic LSM. NASA Tech. Memo. 104606, 58 pp.

Liang, X., and Coauthors, 1998: The Project for Intercomparison of Land-Surface Parameterization Schemes (PILPS) Phase-2c Red-Arkansas River Basin experiment: Part 2. Spatial and temporal analysis of energy fluxes. *Global Planet. Change,* **19,** 137–160.

——, E. F. Wood, and D. P. Lettenmaier, 1999: Modeling ground heat flux in land surface parameterization schemes. *J. Geophys. Res.,* **104,** 9581–9600.

Lundin, L.-C., 1990: Hydraulic properties in an operational model of frozen soil. *J. Hydrol.,* **118,** 289–310.

Mahfouf, J.-F., and J. Noilhan, 1996: Inclusion of gravitational drainage in a land surface scheme based on the force–restore method. *J. Appl. Meteor.,* **35,** 987–992.

McCumber, M. C., and R. A. Pielke, 1981: Simulation of the effects of surface fluxes of heat and moisture in a mesoscale numerical model. *J. Geophys. Res.,* **86,** 9929–9938.

McNider, R. T., A. J. Song, D. M. Casey, P. J. Wetzel, W. L. Crosson, and R. M. Rabin, 1994: Toward a dynamic–thermodynamic assimilation of satellite surface temperature in numerical atmospheric models. *Mon. Wea. Rev.,* **122,** 2784–2803.

Meyers, T. P., and S. Hollinger, 1998: Wintertime surface energy budget within the GCIP domain. *GEWEX News,* **8,** 10–13.

Noilhan, J., and S. Planton, 1989: A simple parameterization of land surface processes for meteorological models. *Mon. Wea. Rev.,* **117,** 536–549.

——, and P. Lacarrère, 1995: GCM gridscale evaporation from mesoscale modeling. *J. Climate,* **8,** 206–223.

——, and J.-F. Mahfouf, 1996: The ISBA land surface parameterization scheme. *Global Planet. Change,* **13,** 145–159.

Pan, H., and L. Mahrt, 1987: Interaction between soil hydrology and boundary layer development. *Bound.-Layer Meteor.,* **38,** 185–202.

Peters-Lidard, C. D., E. Blackburn, X. Liang, and E. F. Wood, 1998: The effect of soil thermal conductivity parameterization on surface energy fluxes and temperatures. *J. Atmos. Sci.,* **55,** 1209–1224.

Philip, J. R., and D. A. de Vries, 1957: Moisture movement in porous materials under temperature gradients. *Eos, Trans. Amer. Geophys. Union,* **38,** 222–232.

Pitman, A. J., Z.-L. Yang, J. G. Cogley, and A. Henderson-Sellers, 1991: Description of bare essentials of surface transfer for the Bureau of Meteorology Research Centre AGCM. Research Rep. 32, BMRC, Melbourne, Australia, 132 pp.

Schlosser, C. A., and Coauthors, 2000: Simulations of a boreal grassland hydrology at Valdai, Russia: PILPS Phase 2(d). *Mon. Wea. Rev.,* **128,** 301–321.

Sellers, P. J., and Coauthors, 1996: A revised land surface parameterization (SiB2) for atmospheric GCMs. Part I: Model formulation. *J. Climate,* **9,** 676–705.

Slater, A. G., A. J. Pitman, and C. E. Desborough, 1998: Simulation of freeze–thaw cycles in a general circulation model land surface scheme. *J. Geophys. Res.,* **103,** 11 303–11 312.

Spans, E. J. A., and J. M. Baker, 1996: The soil moisture characteristic: Its measurement and similarity to the soil moisture characteristic. *Soil Sci. Soc. Amer. J.,* **60,** 13–19.

Thompson, S. L., and D. Pollard, 1995: A global climate model (GENESIS) with a land-surface scheme (LSX). Part I: Present climate simulation. *J. Climate,* **8,** 732–761.

Verseghy, D. L., 1991: CLASS—a Canadian land surface scheme for GCMs. I. Soil Model. *Int. J. Climatol.,* **11,** 111–133.

Viterbo, P., and J.-T. Chang, 1987: Concerning the relationship between evapotranspiration and soil moisture. *J. Climate Appl. Meteor.,* **26,** 18–27.

——, and A. C. M. Beljaars, 1995: An improved land surface parameterization scheme in the ECMWF model and its validation. *J. Climate,* **8,** 2716–2748.

Wetzel, P. J., and A. Boone, 1995: A parameterization for land–cloud–atmosphere exchange (PLACE): Documentation and testing of a detailed process model of the partly cloudy boundary layer over heterogeneous land. *J. Climate,* **8,** 1810–1837.